From the Karolinska Hospital and Institute
Department of Clinical Neuroscience
Section of Clinical Neurophysiology
SE-171 76 Stockholm, Sweden

TRACER DEVELOPMENT AND PET STUDIES: LABELED PROINSULIN C-PEPTIDE AND AN EGFR-TK INHIBITOR

by

Anna Fredriksson

Karolinska Institute,

Stockholm 2002

ABSTRACT

Positron emission tomography (PET), which localizes and quantifies positron decays over time, enables non-invasive in vivo distribution studies of trace amounts of compounds labeled with positron emitters. The use of PET to image disease processes is growing as the number of available tracers increases and, especially, as they become more selective and specific. PET is also increasingly being used in the development of drugs. Since trace amounts of the drug can be administered, distribution and kinetic studies can be performed in humans early in the developmental process to ascertain that the intended biophase is actually reached and to a satisfactory extent and duration.

This thesis includes (1) developments for an imaging approach with oncological application, which is based on an inhibitor of the epidermal growth factor receptor-tyrosine kinase (EGFR-TK) and (2) drug development with respect to studying the pharmacokinetics and biodistribution of proinsulin C-peptide, which is being evaluated for treating long-term complications in type 1 diabetes mellitus (DM).

The EGFR, normally involved in mitogenic signaling, is over-expressed in many different cancer types, e.g. non-small cell lung, glial cell, head and neck, pancreatic, bladder, prostate and breast cancer. A correlation between the amount of EGFR and poor prognosis has been established in a number of these cancers. A radiotracer selective for the EGFR could therefore be of interest for tumor localization and for treatment selection or evaluation of therapeutic response.

Methods to produce a precursor for radiolabeling PD153035 (4-(3-bromoanilino)-6,7-dimethoxyquinazoline), a potent inhibitor selective for the EGFR-TK ($K_i\approx5.2$ pM; $IC_{50}\approx29$ pM), were sought. Synthetic strategies for producing 6- or 7- mono-desmethyl and 6,7-di-desmethyl PD15305 were identified. Thus different positions for labeling can be selected, which is of potential interest for metabolic studies. [6-Methoxy-^{11}C]PD153035 was produced and its in vivo distribution to normal and proliferating tissue was evaluated in rats. In healthy rat, radioactivity was observed mainly in liver, heart, brain and in the gastrointestinal tract. Tumor radioactivity concentrations, studied in rats implanted with a human neuroblastoma cell line (SH-SY5Y), varied in accordance with differences in tumor size and viability (determined post-mortem). The results motivate further studies to determine the selectivity and specificity of [^{11}C]PD153035 distribution to tumor in order to elucidate whether this tracer has potential for EGFR-TK level imaging with PET.

Type 1 (insulin-dependent) DM, characterized by impaired or no insulin production, is accompanied by an increased risk for micro (kidneys, nerves, retina) and macro (heart, brain, extremities) vascular dysfunction. Since insulin is lacking, so is C-peptide, which is normally produced and released in equimolar amounts together with insulin. Studies have demonstrated that administration of C-peptide to IDDM patients results in increased blood flow to skeletal muscle and skin, improved renal function and amelioration of diabetic neuropathy.

A multi-step procedure to label human C-peptide with fluorine-18 based on the activated ester N-succinimidyl-4-[^{18}F]fluorobenzoate ([^{18}F]SFB) to afford N-4-[^{18}F]fluorobenzoyl-C-peptide ([^{18}F]FB-C-peptide) was identified. With the purpose of furthering the knowledge on C-peptide's in vivo distribution, with special emphasis on the kinetics in the kidneys, [^{18}F]FB-C-peptide was studied in monkeys and in volunteering type 1 DM patients using PET. Following iv administration of [^{18}F]FB-C-peptide, radioactivity distributed mainly to the kidneys. A tendency, albeit not statistically significant due to the small number of subjects, to slower kinetics in kidney and liver was observed when pharmacological doses of C-peptide were co-administered with the tracer. Low concentrations of radioactivity in skeletal muscle could, due to their large total mass in the body, account for approximately 15% of the administered dose. The distribution findings are consistent with the documented beneficial effects engendered by C-peptide on renal function and on blood flow to skeletal muscle.

Keywords: PET, imaging, kinetics, oncology, EGFR, PD153035, diabetes, C-peptide

Genom att försöka med det "omöjliga"
når man högsta graden av det möjliga

August Strindberg

Tillägnad Mamma Catharina

PAPERS INCLUDED IN THE THESIS

The thesis is based on the following papers and manuscript (I-VI) and an appendix (App.) with supporting data, which will be referred to in the text by their Roman numerals and with App., respectively.

I.   Johnström P., Fredriksson A., Thorell J.-O. and Stone-Elander S. (1998) Synthesis of [methoxy-^{11}C]PD153035, a selective EGF receptor tyrosine kinase inhibitor. *J. Labelled Cpd. Radiopharm.* **41**, 623-629.

II.   Fredriksson A., Johnström P., Thorell J.-O., von Heijne G., Hassan M., Eksborg S., Kogner P., Borgström P., Ingvar M. and Stone-Elander S. (1999) In vivo evaluation of the biodistribution of ^{11}C-labeled PD153035 in rats without and with neuroblastoma implants. *Life Sci.* **65**, 165-174.

III.   Fredriksson A. and Stone-Elander S. (2002) Rapid microwave-assisted cleavage of methyl phenyl ethers: New method for synthesizing desmethyl precursors and for removing protecting groups. *J. Labelled Cpd. Radiopharm.* **45**, 529-538.

App.   Fredriksson A., Thorell J.-O. and Stone-Elander S. (supporting data) Synthesis of 4-(3-bromoanilino)-7-hydroxy-6-methoxyquinazoline, 7 (7-des-methyl PD150335): Preparation of a reference compound.

IV.   Fredriksson A., Johnström P., Stone-Elander S., Jonasson P., Nygren P.-Å., Ekberg K., Johansson B.-L. and Wahren J. (2001) Labeling of human C-peptide by conjugation with *N*-succinimidyl-4-[^{18}F]fluorobenzoate. *J. Labelled Cpd. Radiopharm.* **44**, 509-519.

V.   Fredriksson A., Ekberg K., Ingvar M., Johansson B.-L., Wahren J. and Stone-Elander S. (2002) In vivo biodistribution and pharmacokinetics of ^{18}F-labeled human C-peptide: Evaluation in monkeys using positron emission tomography, PET. *Life Sci.* (in press).

VI.   Fredriksson A., Ekberg K., Ingvar M., Johansson B.-L., Wahren J. and Stone-Elander S. (2002) In vivo biodistribution of ^{18}F-labeled C-peptide in humans: Evaluation using PET. (manuscript).

Reprints were included with kind permission from the publishers

TABLE OF CONTENTS

ABBREVIATIONS

ATP	adenosine 5'-triphosphate
ca.	circa
c.a.	carrier added
C-peptide	proinsulin connecting peptide
EGF	epidermal growth factor
EGFR	epidermal growth factor receptor
ELISA	enzyme-linked immuonsorbent assay
EOB	end of bombardment
EOS	end of synthesis
FB-C-peptide	*N*-4-fluorobenzoyl-C-peptide
FCS	fluorescence correlation spectroscopy
GF	growth factor
GI	gastrointestinal
HPLC	high-performance liquid chromatography
ip	intraperitoneally
iv	intravenously
LC	liquid chromatography
MAb	monoclonal antibody
MS	mass spectroscopy
n.c.a.	no carrier added
NMR	nuclear magnetic resonance
PD153035	4-(3-bromoanilino)-6,7-dimethoxyquinazoline
PET	positron emission tomography
Rh	rhodamine
ROI	region of interest
SFB	*N*-succinimidyl 4-fluorobenzoate
SPECT	single photon emission computed tomography
s.r.	specific radioactivity
TK	tyrosine kinase
type 1 DM	insulin-dependent diabetes mellitus
% id	percent of the injected dose

INTRODUCTION

Imaging techniques that are based on the external localization of administered radioactivity allow non-invasive and non-perturbed in vivo distribution studies. Positron emission tomography (PET) (1-3) and single photon emission computed tomography (SPECT) (4-6) are two such imaging techniques. Direct tracing of the in vivo location of the radioactivity over time provides information on the labeled molecule's uptake, distribution and regional residence times. Consequently, PET and SPECT supply functional information (7) opposed to the anatomical information provided by other, non-nuclear medicine, imaging techniques including magnetic resonance tomography (MRT), X-ray computed tomography (CT) and ultrasound (US). Such kinetic information is difficult to obtain by other means.

Theory of PET

Positron emitting radionuclides, neutron-deficient isotopes of atoms commonly found in organic matter, form the basis for the PET technique, which is schematically presented in Figure 1. In the decay of the radionuclide, a proton is converted into a neutron with concomitant emission of a positron, β^+. Following emission, the positron collides with its anti-particle, the electron, in the tissue and annihilation occurs producing energy in the form of two gamma photons (511 keV each). The parallel but oppositely directed photons penetrate the body and are externally detected by the PET camera, composed of gamma detectors organized in rings. Simultaneous registration of two photons makes it possible to localize the decay from somewhere along the line in-between the two detectors. Computational treatment of the recorded data provides color-coded images and quantification of the regional concentrations of the tracer.
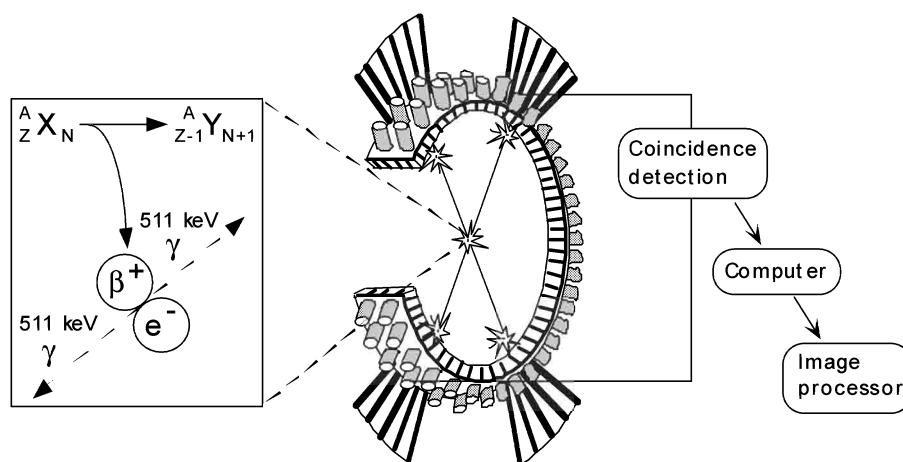

Figure 1. Schematic representation of the principle of PET and a PET camera with the gamma detectors organized in a ring around the study subject.

PET applications

Measurements of changes in tracer concentrations over time in different organs or regions enable estimations of physiological and biochemical processes in normal and pathological states. Parameters relating to blood flow, energy requirements, fatty acid metabolism and amino acid utilization are often analyzed in PET studies. Receptor densities and ligand distribution and binding kinetics can also be assessed.

The areas of PET applications are numerous, but, in addition to the basic research of the past two decades, the following two major categories can be identified: imaging with clinical implications (e.g. (7-11)) and for use in drug development (e.g. (12-17)). The former includes localizing and imaging areas with altered function as, for instance, the changed energy requirements in tumors or epileptic foci. Studies of interactions between receptors and ligands or signal substances, which are believed to be engaged or altered in a wide range of diseases, can also be performed with a number of now well-established radioligands. Response to therapy may be assessed by efficacy evaluations. For example, cancer treatment is expected to decrease tumor glucose utilization, ischaemia therapy to increase blood flow, and psychotherapy to block or activate relevant receptor targets.

PET can provide in vivo information of interest for drug development. A drug's ability to exert its intended action, dependent on the kinetics of its uptake, distribution and residence time in the designated target, can be studied. Even lead compounds identified with in vitro tests and showing promise in animal models may still, after time consuming and expensive evaluations, turn out to be ineffective in humans. The major cause for the failure of new drugs is inappropriate pharmacokinetics (16). Including PET studies early in the developmental process to assess kinetic parameters such as absorption, distribution, metabolism and excretion in humans may lead to faster identification of promising as well as unpromising candidates. The radionuclides used in PET can be produced in high specific radioactivity (s.r.; see Table 1). Therefore, very small amounts of the compound can be administered in "tracer" studies. The risk that the drug will provoke a pharmacological or toxicological effect is minimized and it may therefore be possible, and justifiable, to perform human PET studies early in the screening process. In addition to information on whether or not the kinetics are favorable, drug - target interactions can also be studied. The selectivity and affinity of the drug towards different binding sites can be established. Optimum doses for receptor occupancy can be established, thereby directing dosing protocols for planned clinical trials.

Radionuclides and radiochemistry

The radionuclides most commonly used in PET (Table 1) are short lived and can be produced by nuclear reactions induced by accelerated protons or deuterons (18, 19). The positrons emitted in the decay of the radionuclides have different maximum energies (E_{max}). These energies affect the distance the positron will travel before its annihilation occurs, which in turn, limits the imaging resolution obtainable (20).

When new tracers are to be developed, the radionuclide selected should have a physical half-life that is compatible with the speed of the biological process to be studied. Use of radionuclides with disproportionately long half-lives may lead to unnecessarily high radiation doses. The radionuclides that can be used may also be restricted by the chemical composition of the compound to be labeled, unless making an analog is admissible. Different labeling positions may be more or less attractive, depending on their metabolic degradation pattern, since the PET camera detects radioactivity but does not disclose whether it came from the intact compound or a labeled metabolite. PET investigations are therefore often complemented with studies of radiolabeled metabolites in blood or plasma samples (21).

Radio-nuclide	Half-life (min)	Common production method	E_{max} (MeV)	Max range in water (mm)	Theoretical & (practical) s.r. (GBq/μmol)
^{11}C	20.4	^{14}N(p,α)^{11}C	0.97	4	3.3×10^5 (110-2600)
^{13}N	9.96	^{16}O(p,α)^{13}N	1.20	5	7.0×10^5
^{15}O	2.04	^{14}N(d,n)^{15}O	1.74	8	3.3×10^6
^{18}F	109.8	^{18}O(p,n)^{18}F ^{20}Ne(d,α)^{18}F*	0.64	2	6.3×10^4 (180-3700)

* for production of carrier added [^{18}F]F$_2$, thus with lower s.r. (see discussion below)

Table 1. Physical properties of the radionuclides most commonly used in PET (22, 23).

The short half-lives of the PET isotopes require that the radiotracers are produced rapidly, which limits the number of reaction steps that can feasibly be performed. Synthetic strategies should ideally be designed so that the label is introduced as late as possible and all reaction and isolation steps must be optimized with regard to time, radiochemical yield and s.r. Due to the high s.r., other starting materials and reagents are usually in large excess which may help drive the reaction and increase the incorporation of the radioactivity. Besides the challenge of producing the radiotracer quickly enough in yields sufficient for subsequent in vivo studies, the chemical and radiochemical purity must be high. This is frequently achieved by isolation using

chromatographic techniques such as HPLC prior to the appropriate final formulation. For intravenous injection, the final solution should be sterile and free from pyrogens.

There are many different methods available by which the low molecular form radionuclides obtained from the cyclotron ($[^{11}C]CO_2$, $[^{11}C]CH_4$, $[^{18}F]F^-$) can be converted into compounds with a range of chemical reactivities. Due to the longer half-lives of ^{11}C and ^{18}F (compared to ^{15}O and ^{13}N) more complicated procedures may be permitted (summarized in (24, 25)). Radiolabeling with carbon-11 is commonly based on labeled alkyl halides or alkyl triflates used in alkylations of various substrates including amines, amides, sulfides, carboxylates and alkoxides, and more recently with organostannanes (26). Other ^{11}C-labeled reagents include cyanide, nitromethane, phosgene and different alcohols, carboxylic acids and acid halides.

Fluorine may not be originally present in the compound to be labeled, but in many cases a proton or an alcohol can be substituted by fluorine without causing steric changes. However, changes in the electronegativity and lipophilicity may alter the molecules in vivo characteristics. Most ^{18}F-labeling strategies are based on high s.r. $[^{18}F]F^-$ since $[^{18}F]F_2$ is generally (exceptions in e.g. (27)) produced in low s.r. due to the small amount of carrier added to help recover the produced $[^{18}F]F_2$. Furthermore, $[^{18}F]F_2$ is so reactive that specific labeling is difficult unless it is converted to acetyl hypofluorite (25). Regiospecific electrophilic aromatic fluorinations can be achieved via fluorodemetalation reactions. Aromatic nucleophilic substitutions with $[^{18}F]F^-$ generally require activation by electron-withdrawing groups (NO_2, CN, RCO, CHO, COOR) ortho or para to the leaving group (NO_2, $(CH_3)_3N^+$, $(CH_3)_2S^+$, halogen). Alkyl compounds with appropriate leaving groups are commonly labeled by nucleophilic fluorinations.

Comparison with SPECT

The longer half-lives (hours compared to minutes) of the radionuclides used in SPECT (approximate half-lives, in hours: ^{67}Ga: 78, ^{123}I: 13, ^{131}I: 193, ^{99m}Tc: 6, ^{111}In: 68) improve technique accessibility since the nuclides (or tracers) can generally be transported considerable distances from where they were produced. Usually, the PET-nuclides and tracers are produced at site directly before the investigations, even though limited transportation is possible. Despite these logistical limitations, PET has a number of advantages over SPECT (20, 28). Increased sensitivity and better time resolution make dynamic data acquisition easier and better with PET. Quantification is better due to more accurate methods for attenuation and scatter corrections. Furthermore, the spatial resolution is better in PET than in SPECT (3-10 mm and 8-20 mm, respectively). SPECT, however, allows simultaneous observation of a larger field-of-view than PET ($\approx$ 40 cm and 10-15 cm, respectively), which is an advantage particularly for whole body studies.

OBJECTIVES OF THE THESIS

The overall objective of this research was to develop properly labeled radiotracers and design and perform initial PET studies aimed at providing clinically relevant methods and in vivo information.

The first part (paper I-III, App.) was focused on tumor imaging based on PD153035, which is an inhibitor of the epidermal growth factor receptor tyrosine kinase (EGFR-TK). Since the EGFR is over-expressed in a number of cancer types, a radiotracer allowing non-invasive measurements of EGFR levels may provide a means for cancer staging, therapy monitoring and predictions about which patients would benefit from EGFR-directed therapeutic approaches. The aim of this work was to synthesize a PD153035-based precursor for labeling, radiolabel PD153035 with a positron-emitting radionuclide and preliminarily evaluate its in vivo behavior as the first steps toward developing an EGFR-TK directed radiotracer.

The second part (paper IV-VI) was more drug development oriented and focused on the endogenous proinsulin connecting peptide (C-peptide), which is lacking in type 1 diabetes mellitus (DM) patients. Replacement of C-peptide in these patients has recently been shown to ameliorate long-term type 1 DM complications and this strategy is currently undergoing Phase 2 clinical trials. The aim of this work was to develop a method for appropriately labeling C-peptide with a positron-emitting radionuclide and design and perform PET studies of the in vivo regional distribution and kinetics of the labeled C-peptide.

AN EGFR-TK INHIBITOR FOR TUMOR IMAGING

The EGFR and its implication in oncology

Cellular events such as growth, proliferation and differentiation are mediated via highly regulated networks of signaling pathways. Maintained balance between the action of the growth stimulatory proto-oncogenes and the growth inhibitory tumor suppressor genes is crucial for the prevention of neoplastic transformation. Many of the identified proto-oncogenes exert their normal function at all different levels in the various signal transduction cascades. Growth factors (GFs), which constitute one class of proto-oncogenes, bind to extra-cellular domains of transmembrane receptors thereby triggering intracellular signals, which lead to alterations in the transcription activity.

EGFR structure and function

The epidermal growth factor receptor (EGFR) is a 170 kDa transmembrane glycoprotein that, upon activation, gives rise to different biological responses including mitogenesis or apoptosis, enhanced cell motility, protein secretion and differentiation or dedifferentiation (29). Binding of a GF in the EGF family (e.g. EGF or TGFα) to the extra-cellular N-terminal portion of the receptor leads to activation (schematically represented in Figure 2). Ligand binding causes receptor dimerization, allosteric activation (30), binding of adenosine triphosphate (ATP), activation of the intrinsic tyrosine kinase (TK) (31) and auto-phosphorylation of several tyrosine residues in the C-terminal region. These phosphorylated tyrosine residue hydroxyl groups constitute docking sites to substrates in the signaling cascade on which the receptor TK activity is exerted (reviewed in (32)). Protein phosphorylation and dephosphorylation, catalyzed by protein kinases and protein phosphatases respectively, is recognized as the most important pathway for regulation of protein functions.

EGFR in tumors

EGFRs are present in most cell types, including the nervous system (33), and are expressed in a number of different human tumors. An often cited review by Salomon et al., presents a broad range of tumor types expressing high levels of EGFR as well as the link between over-expressed EGFR and patients with advanced disease, metastases and poor prognosis (34). There are numerous reports indicating that an aberrant expression of EGFRs (or the subtypes) is often correlated with aggressive morphology and poor outcome in different cancer types including non-small cell lung, glial cell, head and neck, pancreatic, bladder, prostate and breast cancer (reviewed in, e.g. (35-37)). The EGFR, also designated ErbB-1, belongs to the ErbB receptor subfamily together with the structurally similar ErbB-2, ErbB-3 and ErbB-4 which also have catalytically active TK domains in the cytoplasmic phase of the cell membrane. Based on over a decade of

clinical and preclinical evidence implicating the EGFR and, more recently, also the ErbB-2, ErbB-3 and ErbB-4, in the development, progression and severity of certain human cancers, this family of receptors has been targeted for the development of anticancer agents. The influence of EGFR level on the degree of malignancy is related to the effects exerted by EGFR on activation of cell motility, cell adhesion, invasion, cell survival and angiogenesis (reviewed in (38)).
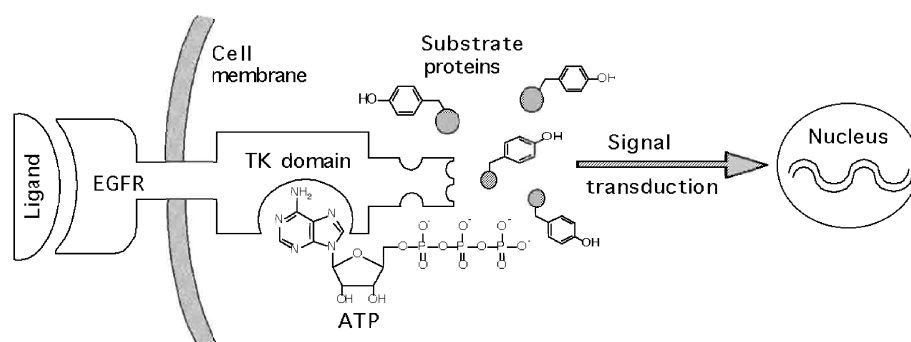

Figure 2. Schematic representation of EGFR structure. Ligand binding, receptor dimerization and kinase activation followed by transfer of the gamma phosphate from receptor-bound ATP to tyrosine residues in substrate proteins involved in signaling pathways leads to altered DNA transcription.

Imaging and therapeutic targets

EGFR as therapeutic target

There are several therapeutic approaches that take advantage of the over-expression of EGFR to target cancer cells, directed both towards the extra-cellular ligand-binding domain and towards the intra-cellular TK domain. The former strategy (the latter discussed below) includes preventing the mitogenic signaling by blocking the ligand-binding region of the receptor with anti-EGFR antibodies (Ab). Ligand-toxin conjugates are also used (39) to bring the toxic agent (or radioactivity for radionuclide therapy e.g. (40), or boron for boron neutron capture therapy e.g. (41)) specifically to the EGFR-rich tumor cells. The ligand-receptor complex is then internalized, thereby exerting its therapeutic effect locally. Using the ligand as toxin carrier can, however, potentially suffer from simultaneous receptor stimulation caused by the ligand-receptor binding. Therefore anti-EGFR Abs are likely to be better carriers (42). As reviewed by Ciardiello, the first agent that specifically interfered with EGFR signaling to enter Phase 2 to 3 clinical evaluation was the chimeric human mouse IgG1 anti-EGFR blocking monoclonal Ab (MAb) IMC-C225 (43).

Imaging based on the EGFR

Clinical applications of PET have been predominantly directed towards oncological investigations (44). The most widely used strategies for tumor imaging (reviewed in (45)), are based on changes in metabolism (using glucose or analogs) and in protein and DNA synthesis (using amino acid or derivatives and DNA binders or precursors, respectively). Based on the increased concentration of receptors in tumors, GFRs have also been recognized as potential targets for mapping and quantification (46).

Since for some tumor types there is a strong correlation between EGFR number and prognosis (invasiveness, response to therapy, survival), quantification of this receptor in diagnosis could facilitate differentiation with regard to therapeutic course and action and result in better patient managment. A suitable radiotracer enabling receptor quantification would allow non-invasive monitoring of changes in levels of receptor expression in response to different therapeutic protocols. Non-invasive characterization of the extent of EGFR expression at the tumor sites could also be used to select patients for therapy directed against EGFR (47-49). For given cancer types (50) high expressers would be candidates for EGFR directed therapy, while low expressers would probably not.

Several nuclear imaging radiotracers directed to the intracellular TK domain (see below) as well as to the extra-cellular domain have been reported in the literature. The latter, MAb, EGF or EGF derivatives, have been labeled with gamma emitters (^{99m}Tc, ^{111}In and $^{125 / 131}$I), e.g. (48, 49, 51, 52). EGF has also been labeled with the positron-emitting radionuclide ^{76}Br (53).

TK inhibitors as therapeutic targets

Since the discovery of the implication of protein TKs in growth processes, studies have been performed on these enzymes and subsequently on strategies to inhibit them in order to find new classes of anti-proliferative agents (54). The fact that over 80% of the oncogenes and proto-oncogenes involved in human cancers code for protein kinases indicate their central role in cancer development (55). Pharmacological inhibition of the signaling pathways would also have potential for treatment of other proliferative diseases as, for example, psoriasis (56). During the past 15-20 years hundreds of compounds have been evaluated in the search for specific EGFR-TK inhibitors (reviewed in (38, 55, 57-59)). Inhibition of TKs can be achieved by two strategies: by ATP competition, or by preventing the TK enzyme substrates from binding. The requirements for TK inhibitors are high potency and, even more importantly, high specificity, since interaction with any of the numerous other membrane-bound or soluble protein TKs could potentially cause severe toxicity. Due to the high degree of structural homology in the ATP binding site in different TKs, the initial work was directed mainly toward substrate competition. However, a breakthrough in potency

achievable came in the mid 1990s with the introduction of the small ATP competitive quinazolines that also possess high selectivity for the EGFR-TK (reviewed in (43, 58, 60)). In 1999 seven small molecule EGFR-TK inhibitors were in early phase clinical trials (61). Six of them are ATP competitive and, of those, three are 6,7-disubstituted 4-anilinoquinazolines (Figure 3). ZD1839 and CP358774 are in clinical trials for oncological applications, whereas PD153035 (Parke-Davis), which was reported to cause apoptosis in tumor cell lines (62, 63), is in clinical trials by Sugen, under the code SU5271, for treatment of psoriasis (55, 64).
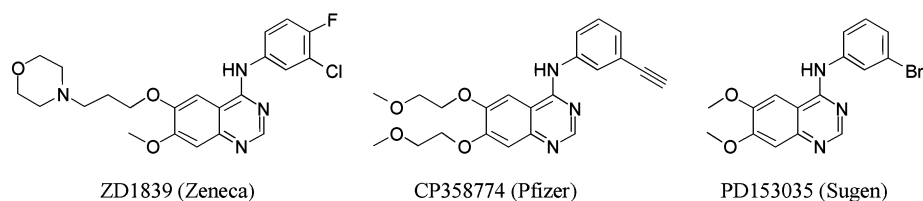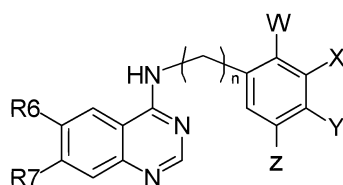

ZD1839 (Zeneca)   CP358774 (Pfizer)   PD153035 (Sugen)

Figure 3. Chemical structures of quinazoline-based EGFR-TK inhibitors under clinical evaluation (the company names given in parentheses).

PD153035 and related quinazoline TK inhibitor radiotracers

In 1994 Fry et al. reported on a new, small molecule, ATP-competitive EGFR-TK inhibitor, 4-(3-bromoanilino)-6,7-dimethoxyquinazoline (PD153035 Figure 3), which had been developed by Parke-Davis (Ltd.) as one in a series of potential chemotherapeutic agents. This compound has an inhibition constant (K_i) of ca. 5 pM which is a three- to five-fold higher affinity than for EGFR-TK inhibitors previously reported (65). Furthermore, PD153035 is unusually selective for the EGFR-TK, which is inhibited to 50% (IC_{50}) at a PD153035 concentration of ca. 30 pM. In tests on activities of isolated recombinant TKs from platelet-derived GFR, fibroblast GFR, colony stimulating factor-1, insulin R and src TK, little effect was detected at PD153035 concentrations as high as 50 μM. Of the six TKs evaluated, only a minor inhibitory effect was observed on the EGFR family member, ErbB-2 TK, with IC_{50} ca. 2 μM. Cell studies (Swiss 3T3 fibroblasts) of the inhibitory effect of PD153035 on EGF induced phosphorylation showed an IC_{50} of ca. 15 nM (65). Other studies showed that the inhibition was very rapid, occurring virtually as the cells (A-431 human epidermoid) were exposed (65). The nature of the binding interaction between the inhibitor and the receptor is suggested to be tight, since cell studies showed prolonged phosphorylation inhibition after removal of PD153035 from the cell medium (65).

The affinity and selectivity of PD153035 for the EGFR-TK make it an attractive candidate for development as an oncological imaging agent. A number of different

analogs of PD153035 have been radiolabeled with positron and single photon emitting radionuclides during the past few years and are summarized in Table 2.

No	R6	R7	n	W	X	Y	Z	Ref.
1	MeO	MeO	0	H	^{123}I	H	H	(66)*†
2	MeO	MeO	0	H	^{125}I	H	H	(66)* (67)†
3	MeO	^{18}F-EtO	0	H	Br	H	H	(68)*†
4	MeO	^{11}C-MeO	0	H	Br	H	H	(68)*
5	^{11}C-MeO	MeO	0	H	Br	H	H	(69)* paper I †
6	MeO	MeO	1	H	H	^{18}F	H	(70, 71)*†
7	EtO	EtO	1	H	H	^{18}F	H	(71)*†
8	MeO	MeO	0	^{18}F	H	Cl	Cl	(72)*† (73)
9	MeO	MeO	0	H	^{18}F	H	CF$_3$	(72)*† (73)†
10	MeO	MeO	0	H	H	^{18}F	H	(73)
11	MeO	MeO	0	H	Cl	^{18}F	H	(74)*† (75)*
12	H$_2$C=CH- ^{11}CO-NH-	H	0	F	H	Cl	Cl	(76)*† (77)*

*   Reported as preliminary abstract or in meeting proceedings.
†   Labeling procedure but not biological (cell line, ex or in vivo) data (other than IC$_{50}$-values in some cases) reported.

Table 2. Radiolabeled PD153035 and analogs

These strategies have directed the label either to the aniline ring or to the 6- or 7-substituents in the quinazoline ring. The ^{11}C-tracers **4** and **5** were produced by *O*-alkylation of the corresponding desmethyl precursors with labeled methyl triflate and methyl iodide, respectively (68, 69, paper I), and **12** by reacting the labeled acryloyl synthon with the amino quinazoline (76). Compound **3** was produced by reaction of ^{18}F$^-$ with the corresponding 7-tosyloxyethyl quinazoline (68). The radioiodinated tracers **1** and **2** were produced by one step iododestannylations of the corresponding trimethylstannyl precursor (66, 67). All the other aniline labeled tracers (**6-11**) were produced by multi-step strategies, in which the appropriate ^{18}F-labeled aromatics were synthesized and then coupled to 4-chloro-6,7-dialkoxyquinazoline (70-73, 75).

In the approach described in this thesis and in paper I, the labeling strategy was chosen so that the drug itself and not an analog would be produced. The structure of PD153035 is particularly well suited for application of the most commonly used strategy for labeling with carbon-11, alkylation of O-, S-, or N- nucleophiles with a prelabeled alkyl halide or triflate (reviewed in (78)). Synthesis of the 6- and/or 7- desmethyl-PD153035 would thus make a one-step radiosynthesis with a routinely prepared labeling precursor possible.

Precursor synthesis, desmethyl-PD153035

Demethylation using BBr3 (paper I)

Reference PD153035 was produced according to the literature procedure (79). Heterocyclization of 2-amino-4,5-dimethoxybenzylic acid with formamide (the Niementowski quinazoline synthesis) was followed by chlorination and subsequent nucleophilic displacement by 3-bromoaniline. Mono-demethylation of PD153035 was achieved with BBr_3 in chloroform at reflux for over 24 h. Although yields were low, the amounts obtained were sufficient for an initial in vivo screening in rats (paper II). A number of other reagents for selective demethylation were tested (80). Of these only $NaSeC_6H_5$ also gave desmethyl-PD153035 in small amounts, but its isolation from the complex reaction mixture was very difficult. Identification of the constitutional isomer produced, was not, at that time, easily accomplished from the available NMR analysis. The product was, however, subsequently determined to be the 6-desmethyl-PD153035 by comparison with the products in paper III and in the appendix. Evidence that the obtained desmethyl product contained only one constitutional isomer was based on HPLC analysis (Figure 6).

Demethylation using MeSO3H - microwave and conventional heating (paper III)

Demethylations are often, as is the case with PD153035, difficult to perform and require stringent conditions and/or long reaction times. Therefore, an alternative approach amenable to the use of microwave dielectric heating was investigated. Microwaves have been used for more than a decade to speed up difficult transformations in organic synthesis (reviewed in (81-83)) and in radiolabeling procedures (reviewed in (84, 85)). Microwave-assisted cleavage of methyl phenyl ethers has previously been performed with pyridine hydrochloride (86), KOBu-*t* and crown ether in ethylene glycol (87), and with lithium iodide and solid supports (88). Here, methanesulfonic acid ($MeSO_3H$) was chosen based on its reported use, together with methionine, in selectively cleaving a methyl phenyl ether (89) and a report that 6-hydroxy-7-methoxy-3,4-dihydro-quinazoline-4-one could be obtained from the 6,7-dimethoxy compound using the same reagents (90). The choice of reagent was further supported by the initial observation that $MeSO_3H$ was very effective at cleaving anisole to phenol in a model reaction. The

a

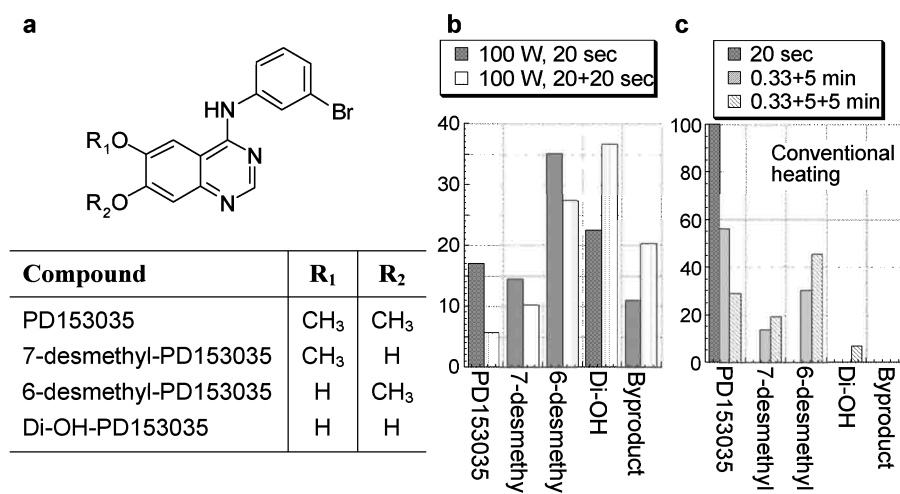| Compound	R₁	R₂
PD153035	CH_3	CH_3
7-desmethyl-PD153035	CH_3	H
6-desmethyl-PD153035	H	CH_3
Di-OH-PD153035	H	H

Figure 4. (a) Chemical structure of the PD153035 and of the products obtained by mono- or didemethylation; (b-c) Diagrams showing the conversion of PD153035 upon heating in MeSO₃H and the product distribution after different reaction times for microwave (b) and conventional (c) heating at 200° C.

polarity of MeSO₃H seemed favorable for a strong interaction with the oscillating electromagnetic field. The high boiling point should, accordingly, mean lower risks for uncontrolled volatilization and containment problems from large pressure increases.

The combination of MeSO₃H and microwaves turned out to be fortunate. Conversions of PD153035 over 80% were achievable in less than a minute of monomodal microwave induced heating. Cleavage occurred at either or both of the methoxy positions giving rise to three products, which were separated on reversed phase HPLC (Figure 6) and identified by LC-MS analysis as the two mono-desmethyl-PD153035 compounds and the di-desmethyl (di-OH) PD153035 (Figure 4a). There was a slight regioselectivity in the demethylation favoring formation of the 6-desmethyl-PD153035 over the 7-desmethyl-PD153035. Prolonging the reaction times consumed more of the PD153035 and the two desmethyl isomers as well, with a concomitant increase of the diphenolic compound and an unidentified hydrophilic byproduct (Figure 4b). Demethylation of PD153035 in MeSO₃H also occurred, but less quickly, using conventional heating. At 200° C ca. 75% conversions were obtained after 10 minutes, but with less diphenol and no byproduct detected (Figure 4c). Consequently, demethylation of PD153035 using MeSO₃H provides a means for rapidly producing the two mono-desmethyl and the di-demethylated PD153035 and thereby the possibility to select the position for the label. Such flexibility may be useful in metabolic studies to establish whether either position is less susceptible to in vivo cleavage and to subsequently label the metabolite for in vivo studies. The rapidity of the microwave-

assisted reaction makes it also potentially interesting for post-labeling removals of methyl group(s), that are often used to protect phenols during aromatic radiofluorinations, e.g. (91).

Synthesis of reference7-desmethyl-PD153035 (App.)

In order to identify which of the two desmethyl-PD153035 compounds were synthesized in papers I and III, one of them, the 7-desmethyl-PD153035, was synthesized by a separate pathway for use as a reference. Applying the original strategy used to produce PD153035 (79), but with the 4-*O*-benzyl protected 2-amino-4-hydroxy-5-methoxybenzylic acid (**13**), 7-desmethyl-PD53035 was selectively obtained as outlined in Figure 5.
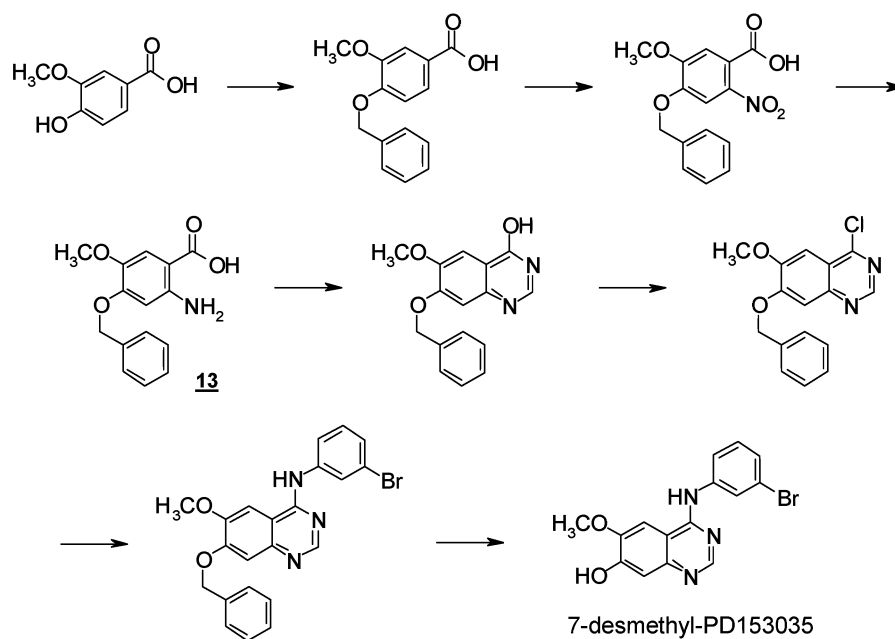

Figure 5. Synthetic pathway used to produce reference 7-desmethyl-PD153035.

Identification of 6- and 7-desmethyl-PD153035

Assignment of the position of the phenol in the radiolabeling precursor (paper I) and in the two mono-desmethyl products (paper III) was based on reversed HPLC analysis. The BBr_3 demethylated precursor co-eluted with one of the $MeSO_3H$ demethylated compounds which were identified by LC-MS, whereas the reference 7-desmethyl-PD153035 co-eluted with the other (Figure 6). Accordingly, the precursor radiolabeled in paper I was 6-desmethyl-PD153035 and the product was [6-methoxy-^{11}C]PD153035 (6-[^{11}C]PD153035).
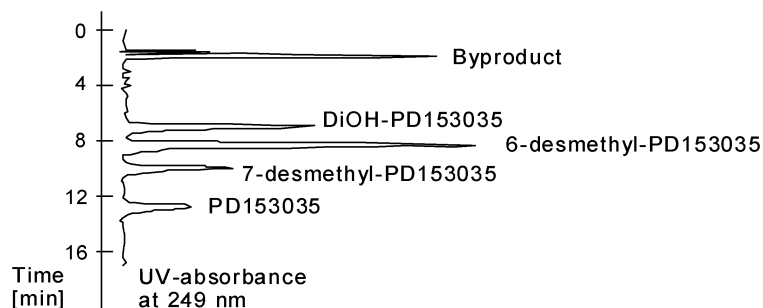
Figure 6. A typical HPLC chromatogram from analysis of the demethylation reactions of PD153035 using MeSO₃H. The constitutional isomers 6- and 7-desmethyl-PD153035 are well separated. The HPLC conditions used were the same as in paper III.

Radiolabeling to produce 6-[^{11}C]PD153035 (paper I)

The alkylation of the phenol group with [^{11}C]methyl iodide (Figure 7), followed by reversed phase HPLC-purification, formulation and sterile filtration, afforded radiochemically pure [^{11}C]PD153035 in a total synthesis time of 45-50 min. According to analytical radio-HPLC the conversion of [^{11}C]methyl iodide to [^{11}C]PD153035 was in the order of 45% using 0.9 mg precursor. At end of synthesis (EOS) the s.r. ranged from 20-40 GBq/µmol (n=7). This s.r. is comparable to that obtained for other ligands labeled in our laboratory using [^{11}C]methyl iodide prepared by the same method (via [^{11}C]methanol produced with lithium aluminium hydride), but for whom precursors have not been generated by demethylation of the targeted reference compound (s.r. at EOS ranging from 5-78 GBq/µmol) (92-94). The s.r. can, if required, probably be increased by a) producing [^{11}C]methyl iodide via the gas phase halogenation of [^{11}C]methane (94, 95), b) reducing the reaction times with e.g. use of [^{11}C]methyl triflate (96), c) starting with [^{11}C]CO₂ of higher s.r. (current cyclotron gives 5-10 times higher). However, considering both the abundant levels of EGFRs and the fact that much larger amounts of PD153035 are tolerated in clinical trials (55, 64), the s.r. obtained here was deemed acceptably high.
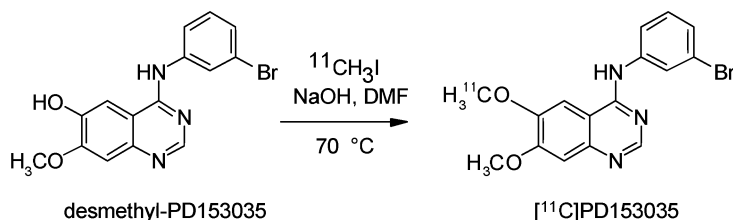

Figure 7. Labeling of PD153035 by alkylation of the 6-desmethyl precursor with [^{11}C]methyl iodide.

In vivo distribution of 6-[^{11}C]PD153035 in rat and tumor implants (paper II)

Organ distribution and dynamics

Following iv administration of 6-[^{11}C]PD153035, the dynamic uptake of radioactivity in different organs in normal rat was studied with PET. Radioactivity was observed in liver, gastrointestinal (GI) tract, lungs, heart and brain. In the lower abdomen (scanned in the tumor bearing rats) radioactivity was observed in testis and in the urinary bladder. Renal clearance was suggested by increasing amounts of radioactivity in the urinary bladder over time. The changes in concentration of radioactivity over time for some of these dynamically scanned organs and for plasma samples taken throughout the study and measured externally in a gamma counter are presented in Figure 8a. For plasma, heart and brain the radioactivity peaked directly in the first sampling and thereafter decreased with beta-phase half-lives of 13 min for brain and heart and 60 min for plasma. The initial extraction of radioactivity from plasma was rapid. The concentration (% of injected dose per mL, % id/mL) at 1 min post injection was only 4% of the radioactivity measured in the first sample (from ca. 15 sec after injection; not shown in Figure 8a).

Distribution to lungs, liver and GI tract was slower and peak values were reached within 2, 4 and 17 min, respectively. After their peaks, the radioactivity concentrations decreased with half-lives of 14, 13 and 21 min, respectively. The amount of radioactivity in the lungs was small (< 0.2% id/mL at max) while concentrations were highest in the liver and the GI tract (excluding the urinary bladder, ca. 1.5-2.5% id/mL at 30 min in the tumor bearing rats). Whether this radioactivity localization is a result of interaction with the EGFRs in the abdomen and/or due to filtration and clearance via the hepatobiliary-intestinal route has not yet been clarified. An ex-vivo study, after administration of the ^{18}F-labeled analog **8** in mice, revealed high uptake in liver and kidneys which was not decreased by preblocking with reference, non-radioactive, **8** (73). The authors presumed that the radioactivity in those EGFR expressing organs was due to rapid metabolism and pre-excretion processing of the tracer and not to specific receptor binding. The observation of high radioactivity concentrations in liver and intestines is, however, also consistent with the findings in other studies targeting the EGFRs in rats, in which the distribution of ^{99m}Tc-labeled humanized MAb against the EGFR and ^{76}Br-labeled mEGF were studied with SPECT (47) and PET, respectively (53).

Distribution to tumor implants

As a first screening study of the distribution of labeled PD153035 to proliferating tissue, PET studies with 6-[^{11}C]PD153035 were performed in three immunodeficient rats (#II-IV) with tumor implants. The rats were subcutaneously injected on the lateral side of the hind legs with SH-SY5Y cells, a poorly differentiated, adrenergic neuroblastoma
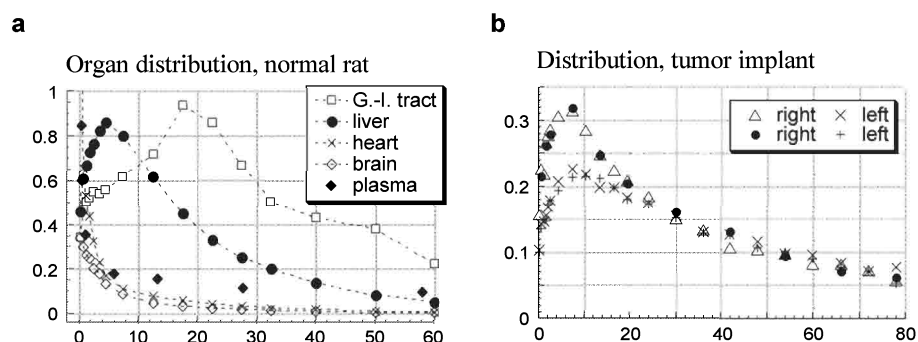
a

Organ distribution, normal rat

Legend: G.-I. tract, liver, heart, brain, plasma

b

Distribution, tumor implant

Legend: right (△), left (×), right (●), left (+)

Figure 8. Time radioactivity curves showing the changes in radioactivity concentration (% id/mL) over time (min) following administration of 6-[^{11}C]PD153035. (**a**) Organ and plasma kinetics in normal rat; (**b**) Radioactivity concentrations in the right and left side tumor implants in rat #II.

cell line capable of anchorage independent growth and xenograft formation. The SH-SY5Y cell line expresses EGFRs (97).

The PET images revealed distribution of radioactivity to all six xenograft sites as shown in Figure 9. The appearance of the activity distribution differed between the sites, from the intense, pronounced in the right side (to the left in the image) of rat #II to the more diffuse in rat #IV. The differences in appearance correlated well with the status of the tumors observed after the PET studies when the tumors were excised for weighing. The weight of each tumor is given directly over the PET-images in Figure 9. In rat #II the tumor sites contained single tumors with the one most distinctly seen in the PET images being considerably larger. The tumors in rat #IV were of comparable weight with that on the right side tumor in #II, but in rat #IV the injected cells had resulted in several, smaller tumors. Since the individual mass of these several tumors was rather small, they had not yet started to grow and divide exponentially and were presumably less viable. Consequently, the less distinct radioactivity in the tumor sites in #IV was consistent with tumor status, but not with measurements of total size.

In the right side of rat #III the uptake was also indistinct despite the large tumor mass. Once again a plausible explanation is related to the viabilibity of the tumors. The tumor growth was followed between xenotransplantation and PET investigation by external volume measurements (with callipers). In rat #III tumor take was established and the tumors grew more quickly than in the other two rats. The right side tumor had passed the phase of exponential growth and was in a stationary or even in a declining phase at the time of the PET study. This lack of viability was confirmed at excision with necrosis revealed in the tumors on both sides. The left side tumor was too necrotic to be removed intact.
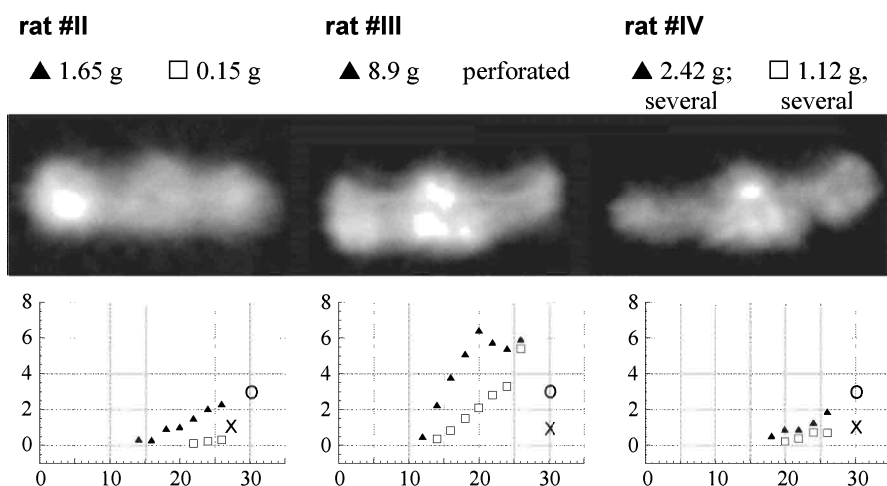
Figure 9. Transaxial images through the tumor implants of the three rats. The xenograft sites on the lateral side of the legs were in proximity of the urinary bladder. The right side tumors are to the left in the PET images and vice versa. For illustrative purposes, the gray scale has been thresholded. Below the PET images, the tumor growth curves are presented, showing the increase in volume (mL) over time (number of days from xenotransplantation) for right (▲) and left (□) side tumors. The day for the PET studies (X) and the day the tumors were excised for weighing (O) are indicated. The tumor weights are given above the PET images.

Regions of interest (ROIs) were delineated over areas corresponding to the tumor implants in several successive transaxial tomographic planes. Time radioactivity curves were obtained which all had a similar pattern of an initial increase followed by a tendency to leveling off and subsequently a slower decrease. Peak levels were reached within 10 min after iv injection. The heterogeneity in the tumor sites also appeared to influence the radioactivity curves. Those for rat #II, presented in Figure 8b, were smooth whereas those for rats #III and #IV were relatively noisy. Morphological inhomogeneity from varying mixtures of viable and necrotic tumor as well as normal tissue may have caused the erratic curves. The amount of radioactivity in all six tumors sites as compared to a reference, non-tumor region drawn over a hind leg in the same rat, was in the order of 15 times higher at peak.

Considerations on the imaging potential of radiolabeled PD153035 or analogs

The study presented in paper II was not designed to demonstrate interaction of the tracer (6-[^{11}C]PD153035) with the EGFR. On the other hand, there are numerous literature reports indicating that the non-radioactive PD153035 interacts with the EGFR in vivo. Dose-dependent inhibition of growth in EGFR over-expressing cell lines (range of

different human carcinoma lines) at low micromolar concentrations of PD153035 have been reported by Bos et al. (62). The inhibitory capacity observed correlated with the degree of EGFR over-expression, i.e. was greater at higher levels of EGFR expression. In another study by Kunkle et al., treatment of tumor implanted (A431 epidermoid carcinoma which over-express EGFR) mice with PD153035 (40 mg/kg, 2 times/day for 5-13 days) did not, contrary to their expectations, provoke any measurable changes in tumor growth (98). They therefore questioned whether PD153035 was affecting its target and examined the EGFR-TK phosphorylation in the tumors. Reduction in phosphorylation was rapid and at 15 min after an ip dose (80 mg/kg) the reduction was as high as 80-90%, relative to controls, which is also indicative of a specific interaction in tumors in vivo.

In spite of the considerable evidence that PD153035 functionally modifies EGFR in vitro and in vivo, it still remains to be conclusively shown that the characteristics of this interaction are favorable for making imaging-based estimates of EGFR levels. The data accumulated to date on the imaging results of radiolabeled PD153035 and analogs are summarized in Table 3. The observations are briefly discussed below, with respect to the radiotracers' dynamic behavior, metabolism and target interactions.

Dynamic distribution to tumor

Of the twelve PD153035-based radiotracers (Table 2), only the distribution of **5** and **8** have been observed dynamically with PET and **1** with SPECT cameras. As discussed in more depth above and in paper II for **5**, radioactivity concentrations in tumor peaked within 10 min at levels ≤ 15 times that in a reference region in leg. Radioactivity levels correlated to tumor status determined post-mortem. Uptake of **8** in mice peaked at 8-12 min though resolution was too limited for a more detailed organ analysis. Dynamic SPECT distribution studies of **1** indicated high uptake of radioactivity in the tumors compared to control tissue. Maximum levels were reached between 30 and 60 min after injection (99).

Radiotracer metabolic stability

To our knowledge, the only studies on the metabolic stability of the radio-PD153035 tracers have been evaluated in animal models with the aniline ^{18}F-labeled analogs of PD153035, **8**, **10** (73) and **11** (75). For **11**, evaluated in normal rat, the ex-vivo organ measurements showed highest retention (6-7% id/g) in the bone. This was taken as an indication of defluorination since non-developing bones have low levels of EGFR and free fluoride is known to be taken up by the skeleton. In the distribution studies with **8** and **10** in tumor (A431) xenotransplanted mice, bone radioactivity was not reported.

No. & Isotope	Model	Study & Unit	Time & Type	Liver	Kidney	G.-I. tract	Urinary bladder	Lung	Brain	Bone	Skin	Heart	Blood/ Plasma	Tumor	Ref.
4 ^{11}C	Mice	ex-vivo % id/g	30 min block[1]	11	5			4.5	0.5				1		(68)*
5 ^{11}C	Rats; normal[2] & tumor model (SH-SY5Y)	PET % id/ml	peak[3] 30 min 60 min	0.86 0.22 0.05		0.93 0.55 0.22	≈ 2 ≈ 1.5 ≈ 2		0.34 0.015 0.004			1.2 0.03 0.007	8.4 0.11 0.10	0.27 0.15 0.08	paper II
12 ^{11}C	Mice; tumor model (A431)	ex-vivo % s.b.[4]	20 min	39.5	13.7						44.5			61.4	(77)*
8 ^{18}F	Mice; tumor model (A431)	ex-vivo[5] % id/g	30 min c.a.[6]	15.3 17.8	20.5 22.7		19.6 40.4	4.94 5.59	2.02 2.75		3.57 7.50	4.25 5.01	4.83 5.88	1.95 3.47	(73)
10 ^{18}F	Mice; tumor model (A431)	ex-vivo % id/g	30 min 60 min	2.3 0.97	3.59 1.47			2.24 0.9	0.21 0.14		1.56 -	1.94 0.81	1.89 0.79	1.14 1.34	(73)
11 ^{18}F	Mice	ex-vivo % id/g	several points[7]	high		high				6-7					(75)*
1 ^{123}I	Rats; tumor model (13762 MAT)	SPECT	high radioactivity uptake in tumor compared to control; t_{max} 30–60 min												(99)*
2 ^{125}I	Cells (MDA-468)	in vitro	specific binding; allosteric activation by EGF												(66)*

* Reported as preliminary abstract or in meeting proceedings.
1.) blocking experiments (5 mg/kg i.p.) caused 50-100% compared to control
2.) values reported are for the normal rat, except for the tumor, urinary bladder and testis: peak levels (≈ 0.15) within ca 10-30 min, at 60 min < 0.1
3.) values at peak concentration; tumor value reported as mean of left and right side for rat #II
4.) s.b.: specific binding
5.) PET study performed, t_{max} in xenograft region ca 8-12 min post injection
6.) c.a.: carrier, non-radioactive **8** co-administered in 500 times molar excess compared to tracer; values reported are from 30 min post injection
7.) measurements made at 2, 5, 20 and 90 min; highest level observed in bones thus defluorination concluded

Table 3. Summary of available data, including organ radioactivity levels, from evaluations of the PD153035-based radiotracers.

The metabolite analysis performed by Bonasera et al. indicated a rapid in vivo degradation of both **8** and **10**. The ^{18}F-analogs (**8**, **10** and **11**) of PD153035 labeled in the aniline ring were thus not considered promising candidates for in vivo EGFR studies.

Receptor - radiotracer interactions

Specific interaction of the radioiodinated **2** has been demonstrated in vitro in EGFR rich MDA-468 cells since pretreatment with PD153035 blocked the radioactivity uptake by 75% (66). Furthermore, the radioactivity uptake was increased up to 9-fold by co-incubation with EGF, which indicted an allosteric activation of the binding site.

In ex-vivo studies of **4** (7-[^{11}C]PD153035) in normal mice, specific uptake could not be demonstrated at 30 min post injection (68). Pretreatment with PD153035 (ip 5 mg/kg) resulted instead in a 50-100% increase in radioactivity content in the sampled tissues. An explanation for these findings was not given. The authors speculated though, that one possible reason could be that the EGFR levels in normal tissues are too low to detect with this kind of protocol (68). Most normal cell types express 20,000-50,000 EGFRs per cell whereas some cancer cells express as many as over 1,000,000 EGFRs per cell (100). Considering the large amounts of endogenous ATP (59, 101) the amounts of PD153035 used may not have been high enough to have significantly blocked the EGFR-TK sites for the radiotracer. However, the dynamic distributions observed with **5** suggest that a more optimal time for examining blocking effects might have been at ca 10 min post administration.

The ex-vivo biodistribution studies performed with **8** and **10** in tumor bearing nude mice demonstrated neither high nor specific binding in the EGFR rich tumor (73). Blocking studies performed with **8** did not conclusively decrease radioactivity concentrations in organs measured ex vivo. It was discussed that these results could be affected by unfavorable kinetics of e.g. receptor-radiotracer association and dissociation and rapid blood clearance. Rapid plasma clearance due to too fast association of the radiotracer with the receptor might potentially result in a measure of blood flow rather than of receptor concentrations (102). However, once again, perhaps a more optimal time to examine the binding would have been during the first 10 min after tracer administration. The Israeli group concluded that the non-specific distribution observed with the ^{18}F-labeled analogs would have to be eliminated to achieve better imaging. They turned towards the acrylamide substituted quinazoline **12** based on literature reports on similar compounds which inhibit the EGFR-TK rapidly and irreversibly (103). The irreversible interaction between the radiotracer and the EGFR-TK would possibly suffer less from competition with the endogenous ATP. In a recent preliminary communication on **12**, ex vivo measurements at 20 min after tracer injection indicated specific binding of radioactivity in tumor as well as in skin, liver and kidneys (77). The

combination of a longer tracer-target interaction and an earlier measurement time was apparently favorable for observing the specific interaction.

Potential for further studies with 6- or 7-[^{11}C]PD153035

We consider our results obtained with 6-[^{11}C]PD153035 (**5**) in paper II as promising. As pointed out above, distribution of radioactivity to regions known to express high levels of EGFRs (liver, GI tract) as well as to regions coupled to cancer types with EGFR over-expression (lung, head, brain, bladder) has been studied. At times later than ca. 5-10 min following tracer administration, high levels of radioactivity were, for the organs studied, exclusively observed in liver and in the area of the GI tract. Highest amounts of radioactivity in the tumor sites was reached within the first 5-10 min. The amounts of radioactivity in the different xenograft sites also correlated well with the status of the tumors observed on excision. However, the study was not designed to investigate specific interaction between tracer and EGFR. Attempts at dose-dependent blocking or displacement of tracer retention or interaction, possibly in another animal model, would be a feasible next step in the tracer validation.

Another aspect to examine is the in vivo metabolism of the labeled tracer. Formation and recirculation of radioactive metabolites can confound the time radioactivity data and make pharmacokinetic modeling more complex (21). Metabolite studies were not performed in our 6-[^{11}C]PD153035 experiments and thus information on the metabolic pattern of trace amounts of the compound in the time span of a PET investigation with carbon-11 is not available. Both 6- and 7-desmethyl-PD153035 have been detected in blood after administration of large doses of PD153035 (80 mg/kg) to mice (98). However, neither the extent nor the time-course for the appearance of those metabolites was reported. Both demethylated compounds have a high affinity for the EGFR (K_i 25-170 pM compared to 5 pM for the parent compound). Thus even the labeled metabolite might maintain a receptor interaction. Since the didemethylated compound was not detected (98), an optimization with regard to labeling in position 6- or 7- might be fruitful. In the radiotracer experiments with **8** (73), the didemethylated metabolite was only found in liver and kidney extracts and not recirculating in the blood.

For imaging purposes a radionuclide with fairly short half-life is suggested. Distribution of PD153035 to tumors in mice was rapid with peak levels reached within 15 min after ip administration (98). Nor have the results obtained in our initial animal studies (paper II) yet suggested the use of a radionuclide with longer half-life than ^{11}C. Blood clearance was rapid, peak levels of radioactivity in the tumor regions were reached within 10 min and the washout phase had a half-life of ca. 40-45 min. Mishani et al. also suggested that the shorter physical half-life of carbon-11 might be more appropriate

than fluorine-18 for the in vivo imaging (76). Distribution and metabolism as well as kinetic patterns may, however, vary considerably between humans and non-human primates, a factor which has not only affected predictions about tracer imaging capacity, but therapeutic results with experimental drugs as well. Further studies are therefore motivated to evaluate whether [^{11}C]PD153035 has potential for EGFR level imaging in humans.

PROINSULIN C-PEPTIDE LABELED FOR DISTRIBUTION AND KINETIC STUDIES

Diabetes mellitus

Diabetes mellitus (DM) is characterized by chronic hyperglycemia resulting from impaired or abolished insulin production in combination with varying degrees of insulin resistance. Insulin is produced by the beta-cells in the pancreatic Langerhans islets and is released in response to increased blood glucose levels. Insulin promotes an increase in glucose transport primarily in the liver, muscle and adiopose cells. Other effects of insulin include increased synthesis (and concomitant decrease in breakdown) of glycogen, fatty acids (lipids) and proteins.

There are two main types of DM, the type 1 insulin-dependent and the type 2 non insulin-dependent DM. Type 1 DM is an autoimmune disease characterized by selective destruction of the insulin producing beta-cells in the pancreas which ultimately leads to a discontinuation of insulin production. Type 1 DM can occur at any age, but most typically in children or adolescents. Type 2 DM is often associated with marked insulin resistance in combination with a gradual decline in insulin production due to impaired beta-cell function. Type 2 DM may also eventually become insulin-dependent. The type 2 DM is the most common form, constituting ca. 85-90% of all DM patients. Notwithstanding, there are ca. 44,000 patients with type 1 DM in Sweden of whom about 50% will, or already have, developed the complications associated with type 1 DM (104). The yearly incidence of type 1 DM in Sweden is ca. 14 (all ages; 30 for people < 15) new diagnosed patients per 100,000 inhabitants (105).

Long-term complications type 1 DM

Patients with type 1 DM are at high risk of developing micro- and macrovascular complications. The complications involve the peripheral and autonomic nerves, the kidneys, the retina and the peripheral arteries (105). Neuropathy is related to lower extremity impairments such as limited function and walking abilities and diminished sensory function. In addition to the chronic pain often experienced by DM patients with neuropathy, lower limb amputation may even become necessary (106). The nephropathy, proceeded by a phase of glomerular hyperfiltration, starts with micro- and macroalbuminuria and is followed by decreasing glomerular filtration. The retinopathy may lead to blindness.

There is no single postulated underlying mechanism responsible for the pathogenesis of the different long-term complications. They are rather thought of as arising from a complex interplay of multiple interactions (reviewed in (107)). One of the major causes is thought to be due to the so-called advanced glycosylation end-products (AGE)

formed by reaction of glucose with amino groups of proteins. The AGEs interact with adjacent proteins to form stable crosslinks, reducing the elasticity in the tissues. Alteration of cellular redox potentials, hypoxia and generation of reactive oxygen species, reduction in Na^+,K^+-ATPase activity and impaired blood flow as a consequence of (among other things) perturbed nitric oxide metabolism have also been implicated in the development of the long-term complications.

Strategies for treatment of the complications

DM treatment strategies include normalization of blood glucose levels and prevention of long-term complications. The former may be achieved by better glucose level monitoring (continuous), by improved devices for maintaining glucose homeostasis and optimal or stimulated insulin dosing (e.g. formulation for appropriate release speed, insulin prodrugs or analogs with favorable kinetics, agents capable of preserving beta-cell function, insulin secretion stimulators) (108). Approaches for preventing specific complications include the use of vasodilators to increase the blood flow and counteract hypoxia in nerves, agents to capture reactive oxygen species (106) and agents that can reverse (cleave) the AGE crosslinked proteins to restore the vascular system (109).
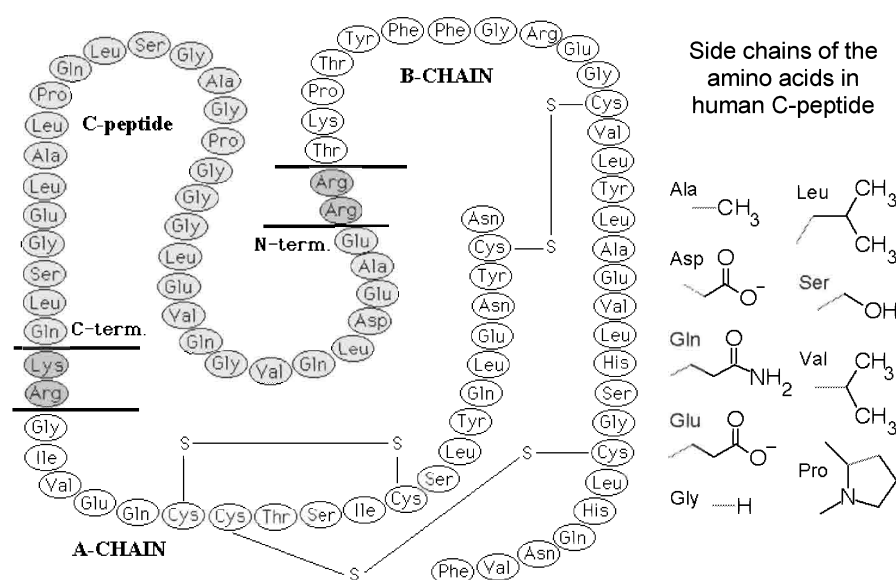

Figure 10. Structure of proinsulin with the A and B chains of insulin and the 31 amino acid large C-peptide.

C-peptide

Insulin is composed of two polypeptide chains (A and B) held together by cystine bridges. However, in the biosynthesis of insulin a single polypeptide chain, preproinsulin, is produced. This precursor protein is cleaved to proinsulin and transported from the endoplasmic reticulum to the Golgi apparatus for storage. Proinsulin is subsequently enclosed in secretory granules and the C-peptide connecting the insulin A and B-chains (Figure 10) is cleaved off. C-peptide and insulin are thus released into the blood circulation in equimolar amounts.

Effects of C-peptide in type I DM

After the discovery that the biosynthesis of insulin proceeds via the larger precursor protein (110), C-peptide was for long considered to possess little, if any, biological function other than bringing the A and B chains of insulin together to facilitate formation of the two cystine bridges. However, recent studies (reviewed in (111-113)) on C-peptide administration to type 1 DM patients, who have no insulin production and accordingly lack C-peptide, report positive effects on and amelioration (even normalization) of long-term complications. The majority of the described benefits are on renal and nerve function. Decreased glomerular hyperfiltration (114, 115) and urinary albumin excretion (116), as well as improved sensory (116, 117) and autonomic nerve function (116, 118) have been observed. Other demonstrated effects include improved oxygen and glucose metabolism in skeletal muscle (114, 119) and improved microcirculation in skin (120), skeletal muscle (119) and myocardium (121). Generally, no effects have been observed when C-peptide has been administered to healthy subjects.

Mode of action

The mechanism by which C-peptide exerts its physiological effects is now emerging. In the search for biological systems affected by C-peptide, endothelial nitric oxide synthase (eNOS) and Na^+,K^+-ATPase have been investigated since their activity is reduced in nerve and kidney tissue in type 1 DM. Both have been found to be activated by C-peptide, reviewed in (113). In vitro studies performed on endothelial cells indicate that C-peptide increases the Ca^{2+} influx and elicits a specific activation of eNOS (122). An increased level of NO might explain the vasodilating effect of C-peptide observed in vivo (123). Several reports provide evidence for the Na^+,K^+-ATPase stimulatory effect of C-peptide (124-126). Findings from in vitro studies on tubules dissected from rat kidneys indicate that the Na^+,K^+-ATPase stimulation also proceeds via a Ca^{2+}-dependent intracellular pathway, possibly activated by a G-protein coupled receptor (127). The C-peptide stimulation of Na^+,K^+-ATPase is concentration dependent (127).

In an in vitro model (skin chamber granulation tissue model) Ido et al. investigated the structural features critical for C-peptide to mediate its effects on glucose induced vascular dysfunction (124). Activities of synthetically produced reverse C-peptide as well as all-D-amino acid C-peptide in this in vitro model were comparable to that of native C-peptide. These observations suggested that C-peptide's effects on vascular dysfunction might be mediated by interactions that are nonchiral and independent of peptide bond direction, rather than by stereospecific receptors or binding sites.

Another study performed in vitro by Rigler et al. using fluorescence correlation spectroscopy, FCS (128), indicated stereospecific binding of C-peptide to membranes, possibly to a G-protein coupled receptor (129). The study, based on fluorescently labeled rhodamine-C-peptide (Rh-C-peptide, Figure 11), showed specific binding of the labeled C-peptide to human renal tubular, fibroblast and endothelial cells. Treatment of the cells with 1,000-fold molar excess of native human C-peptide displaced the Rh-C-peptide to 85%. Binding decreased in the same order of magnitude by preincubation with native C-peptide. The biologically active C-terminal pentapeptide, in 1,000-fold molar excess, also displaced the Rh-C-peptide by approximately 85%. Binding to renal tubular cells was saturated at nanomolar concentration of the Rh-C-peptide (0.9 nM) and 50% binding was obtained at ca. 0.3 nM. The binding was specific since neither C-peptide with all-D-amino acid nor insulin, proinsulin or the insulin-like GFs I or II displaced the bound, Rh-C-peptide.

Distribution and kinetics

The distribution of C-peptide in humans has not been fully described but a number of observations have contributed to the current understanding. Evidence has been presented that the kidneys are the major sites for uptake and catabolism of secreted as well as administered C-peptide. Approximately 30-50% is eliminated via the kidneys, primarily by renal degradation (130, 131). Only a small portion, 3-5%, is secreted as intact C-peptide to the urine (131) and the hepatic extraction appears to be negligible (131-133). Little information is available on extra-renal sites of C-peptide catabolism. However, measurements of arterio-venous differences of C-peptide across the forearm vascular bed has suggested binding of the peptide to the vascular bed or uptake to the muscle tissue (119). The half-life of C-peptide in plasma is 30-40 min and tends to be longer in patients with type 1 DM (131, 134).

Purpose of C-peptide PET studies

C-peptide is currently undergoing Phase 2 clinical trials for prospective introduction as a therapeutic agent for preventing or retarding the development of the long-term complications in type 1 DM. PET enables the regional study of the localization and

pharmacokinetics of labeled compounds. PET is increasingly used in drug development to obtain information about how much of the administered drug that is reaching the target/effector site(s) in healthy and diseased tissues, the rates governing its concentration in each target tissue, and the factors influencing its elimination via renal or hepatobiliary clearance. This kind of information might help further the knowledge about site(s) of C-peptide action, metabolism and secretion. We therefore sought to label the peptide in a way that would minimally perturb its structure and examine the distribution first in a screening study in animals and then in type 1 DM subjects. The primary focus was on organs that C-peptide is known to influence positively, the kidneys and the heart. The capability of simultaneously examining for other possible localization sites was clearly of interest.

Methods to label peptides for PET or SPECT

Peptides (and proteins) can be radiolabeled in various ways, depending on both the selected nuclide and on the characteristics of the peptide. Radiometals (135) can only be attached by chelation (136). Either the chelating agent is covalently bound to the peptide prior to labeling, or the chelate-radiometal complex can be first formed and then conjugated to the peptide.

Methods for radiohalogenating proteins have been extensively reviewed by Wilbur (137). Direct oxidative radioiodination is a straightforward technique applicable with several functional groups commonly present in proteins. If, however, the appropriate amino acids are lacking or if the protein is sensitive to the oxidative conditions, a prosthetic group might be used for conjugate labeling. The prosthetic group can, as with the chelating agents, be labeled either before or after being covalently conjugated to the peptide. In the former strategy, which permits harsher reaction conditions in the labeling steps, acylation, alkylation, amidation or photochemistry have been used to achieve the conjugation. The latter strategy, advantageous since only one radiolabeling step will give higher radioactivity yields and better s.r., requires however that the prosthetic group is activated enough for direct labeling.

A few reagents have been used to label proteins with carbon-11. Reaction conditions can be relatively mild and several functional groups have been targeted (138).

Radiolabeling of human C-peptide (paper IV)

Selection of labeling strategy

A labeling strategy causing a relatively small change in the native C-peptide was desirable. Unfortunately, the amino acid content of human C-peptide (Figure 10) does not lend itself to direct radioiodination (i.e. no aromatic residues). A chelated radiometal might be large enough to influence both the distribution and the kinetics of this

relatively small peptide. A prosthetic group may, of course, alter in vivo behavior but, contrary to a co-ordinated metal a covalently attached group is not subjected to competition from serum cations or the risk for simple translocation of the label to blood proteins e.g. albumin and transferrin (135).

Fluorine-18 was selected for labeling the prosthetic group due to the good imaging properties of ^{18}F and since its physical half-life is suitable for the process to be studied (reported half-life of C-peptide in plasma around 30-40 min). Furthermore, of the halogens fluorine forms the strongest bond with carbon (bond energy: F > Cl > Br > I > At). Thus the risk for in vivo dehalogenation should be less for a ^{18}F-labeled group.

The drawbacks and advantages of different prosthetic group strategies for ^{18}F-labeling of peptides have been reviewed in (139, 140). Activated esters of *N*-hydroxysuccinimide are good electrophiles for conjugation to nucleophiles, such as amines, to form stable amide bonds. *N*-Succinimidyl 4-[^{18}F]fluorobenzoate ([^{18}F]SFB, Figure 12), an analog of the prosthetic group developed by Bolton and Hunter in 1973 for radioiodination of proteins (141), has been successfully developed for PET radiolabeling (142-146). Smaller acylation agents like activated fluoropropionyl have been used and also compared to [^{18}F]SFB (143). The observed peptide conjugation potential for [^{18}F]SFB is more favorable (143) and the aromatic fluoride bond of [^{18}F]SFB is, furthermore, presumed to be more stable. [^{18}F]SFB was less sensitive to competing hydrolysis and gave higher aminolysis yields. Acylation of proteins with [^{18}F]SFB has also been reported to be superior to photochemical conjugation (using 4-azidophenacyl-[^{18}F]fluoride) with regard to both conjugation yields and to in vivo stability (146).

Based on the considerations above, [^{18}F]SFB was selected for the prosthetic group labeling of C-peptide even though several radiochemical steps are required for its production. If concerns about aliphatic defluorination can be allayed, the analogous *N*-Succinimidyl 4-[^{18}F](fluoromethyl) benzoate can alternatively be produced in a single fluorination step with a tosyl leaving group (147, 148).

Retained interaction in vitro

The radiolabeling strategy using [^{18}F]SFB was selected based on predictions that the peptide characteristics would be minimally perturbed. Studies on the activity inherent to different fragments of C-peptide have indicated that the N-terminal portion is less important for its biological activity. A pentapeptide identical to the C-terminal elicits approximately the same stimulation of Na$^+$,K$^+$-ATPase as the entire C-peptide, whereas the corresponding, N-terminal, segment of 26 amino acids possesses almost no activating capacity (149). Peptide fragments of different lengths corresponding to the mid-segment of C-peptide retained between 35-80% of the stimulatory effects of the

native C-peptide. Furthermore, Ido et al. reported that nonpolar amino acids in the midportion of the peptide were required for C-peptide's effects on glucose-induced vascular dysfunction (124). A fragment lacking 3 amino acids in the N-terminal and 7 in the C-terminal retained almost full activity. [^{18}F]SFB, a good electrophile, is known to react preferably with primary amines such as the ε-amino groups of lysine (146). Since human C-peptide does not contain lysine (or other amine functions), conjugation with [^{18}F]SFB results in site-directed labeling in the N-terminal giving *N*-[^{18}F]fluorobenzoyl-C-peptide ([^{18}F]FBC-peptide), with the prosthetic group separated from the portions documented to be active.

Cell membrane interaction capacity of synthesized, non-radioactive, reference FB-C-peptide was evaluated by FCS. With FCS the Brownian movements of molecules, labeled with a single fluorescent group, can be studied at the level of the cell membrane. Following excitation by a laser beam, the fluorescence emitted from a small volume (0.2 fL) in the level of the cell membrane or in the incubation media is recorded (128). The intensity of the recorded signal is proportional to the number of molecules in the focused volume. Emission fluctuations over time reflect the diffusion times for the molecules at the cell membrane or free in the medium. The mathematically assessed diffusion times reveal interactions, since the diffusion velocities tend to be slower for larger compounds or complexes.
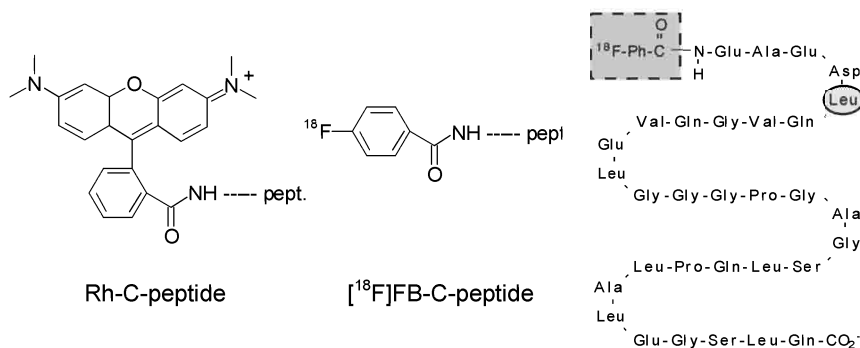

Figure 11. Chemical structure of rhodaminyl- and fluorobenzoyl- groups and their covalent linkage to peptide (= pept) N-terminal. Schematic drawing of FB-C-peptide, showing the relatively small change of the native structure produced by the fluorobenzoyl group. The monkey C-peptide only differs from the depicted human C-peptide in one single amino acid, i.e. the encircled leucine which is proline in the monkey peptide.
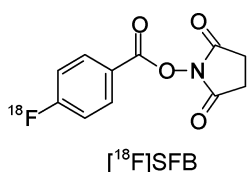
Similarly to the FCS and C-peptide studies mentioned above (129), C-peptide labeled in the N-terminal with tetramethyl-rhodamine (Rh-C-peptide) was used to evaluate FB-C-peptide. Rh-C-peptide binds specifically to cell membranes similarly to native C-peptide since the binding can be blocked and displaced to ca. 85% by native C-peptide.

The FCS studies using renal tubular cells indicated that FB-C-peptide blocked and displaced the binding of Rh-C-peptide to ca. 80% (unpublished data, personal communication A. Pramanik). Indirectly, this implies that FB-C-peptide cell membrane interactions are very similar to those of native C-peptide. That conclusion is further strengthened by the fact that the C-terminal pentapeptide in itself interacts with the cell membranes as strongly as the entire peptide (129) and that the structural alteration of the specifically binding Rh-C-peptide is larger than that of FB-C-peptide (Figure 11).

Labeling of human C-peptide with [^{18}F]SFB

[^{18}F]SFB was produced by nucleophilic radiofluorination (with non carrier added, n.c.a., [^{18}F]F$^-$) of 4-trimethylammonium-benzonitrile, hydrolysis of the nitrile to [^{18}F]fluorobenzoic acid for reaction with N,N'-disuccinimidyl carbonate, via a slight modification of literature procedures (142, 143, 145). Starting from resolubilized [^{18}F]F$^-$ (4.8-8.2 GBq, n=4), [^{18}F]SFB was produced in 45-58% isolated (HPLC), decay-corrected yields after ca. 155 min. [^{18}F]SFB was isolated by HPLC because previous studies have indicated that the peptide coupling efficiency is lower when only solid phase extraction is used (144). C-peptide is a rather small and hydrophilic peptide, which may have influenced its reactivity towards SFB. It did not react readily even when a large excess of unlabeled SFB was used to synthesize reference FB-C-peptide. The reaction conditions were optimized for reproducible and reliable labeling of C-peptide (Figure 12). Conversions of [^{18}F]SFB to [^{18}F]FB-C-peptide (based on radio-HPLC analysis) and HPLC-isolated, decay-corrected yields of ca. 20-25% and 17-21%, respectively, were obtained using a large excess of C-peptide to drive the conjugation. HPLC purification of [^{18}F]FB-C-peptide was necessary to remove the excess of unreacted peptide and radioactive by-products, such as [^{18}F]fluorobenzoic acid, formed by competing hydrolysis. That the unreacted C-peptide was successfully removed was indicated by the fact that the end of bombardment (EOB) s.r. of the [^{18}F]SFB and of the [^{18}F]FB-C-peptide estimated by radio-HPLC and by ELISA, respectively, were of same magnitude. The [^{18}F]FB-C-peptide produced, in a total synthesis time of less than 5h and in a decay-corrected radiochemical yield of 8-12% based on resolubilized [^{18}F]F$^-$, had a s.r. of 25-130 GBq/μmol at the time of injection for the PET studies (concentrations estimated with ELISA). These values recalculated to EOB, are consistent with those obtained in other radiolabelings performed with the [^{18}F]F$^-$ produced with the Scanditronix MC 16 cyclotron and ^{18}F-target used here, e.g. (150).

The amounts and s.r. of [^{18}F]FB-C-peptide could probably be improved by several measures. The synthesis time for [^{18}F]SFB could be shortened using *O*-(*N*-succinimicyl) *N,N,N',N'*-tetramethyluronium tetrafluoroborate (TSTU) to convert the [^{18}F]fluoro-benzoic acid (146). In addition to short reaction times, this reagent possesses ionic features that facilitate purification with solid phase extraction. Furthermore,

pH	n	MeCN	DMF
7.5	1	18.2	20.8
7.7	3	21.0-25.4	14.9-19.4
8.4	2	6.9-10.1	7.5-10.9
8.7	1	5.2	4.6

[^{18}F]SFB

Figure 12. Structure of [^{18}F]SFB and its conversion (expressed in %) to [^{18}F]FB-C-peptide in borate buffer of different pH and with (20%) acetonitrile or dimethyl formamide added.

automation of the synthesis would allow the use of larger quantities of starting radioactivity.

The amounts and s.r. of [^{18}F]FB-C-peptide could probably be improved by several measures. The synthesis time for [^{18}F]SFB could be shortened using O-(N-succinimicyl) N,N,N',N'-tetramethyluronium tetrafluoroborate (TSTU) to convert the [^{18}F]fluoro-benzoic acid (146). In addition to short reaction times, this reagent possesses ionic features that facilitate purification with solid phase extraction. Furthermore, automation of the synthesis would allow the use of larger quantities of starting radioactivity.

Other more recent strategies that have been used to speed up the labeling procedure include the use of microwaves both in the production of [^{18}F]SFB (e.g. in the initial nucleophilic aromatic fluorination of the quaternary salt (151, 152)) and in the peptide conjugation reaction (153), use of other reagents allowing the direct coupling of [^{18}F]fluorobenzoic acid to the peptide (152, 154), use of solid phase supports to facilitate the isolation of the labeled peptide (154), or a combination of all of these might be possible (155).

PET distribution studies of [^{18}F]FB-C-peptide

Monkey studies (paper V)

PET distribution studies were initially performed with [^{18}F]FB-C-peptide in two *Cynomolgus* monkeys (#I and II) that had fasted overnight in order to minimize the levels of released insulin and C-peptide. The monkeys were anesthetized and placed on their back with a selected body segment (#I: chest dynamically, 0-60 min; #II: abdomen dynamically 0-116 min and static head, ca. 120-130 min) in the PET camera's field-of-view. Following iv tracer administration (ca 3 MBq/kg), the radioactivity distributed mainly to the kidneys and, to a lower extent, to the heart and liver (#1, Figure 13a). Within the kidneys, the radioactivity located first in the cortex and subsequently to the pelvis. Urinary excretion of the radioactivity was observed. The radioactivity concentration increased drastically ca. 10 min after injection and leveled off at ca. 10% id/mL (#2, Figure 13b). The lower abdomen scan (#2, female) revealed no other high

radioactivity regions than the kidneys and the urinary bladder. Nor did the late scan over the head reveal any appreciable levels of radioactivity within the brain (#2). Time-radioactivity curves for kidney, heart, liver and urinary bladder are shown in Figure 13b.
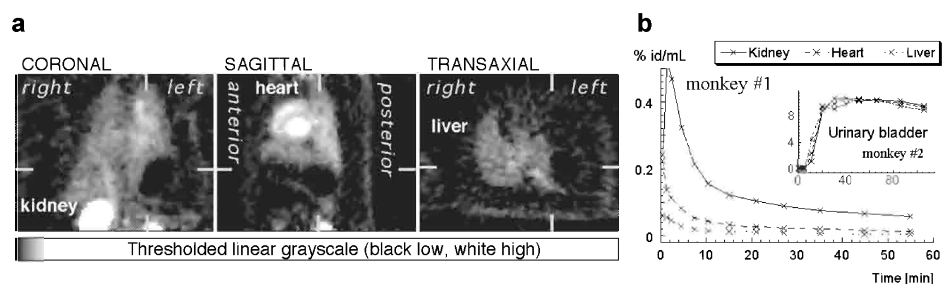

Figure 13. (a) PET image showing the distribution of radioactivity in the chest of monkey #1 following administration of [^{18}F]FB-C-peptide. (b) Diagram with the variation of radioactivity over time for the organs with most distinct levels of radioactivity (#1) and for the urinary bladder (#2).

The objective of these monkey screening studies was to obtain information on the general pattern for [^{18}F]FB-C-peptide distribution with time. This information formed the basis for the design of the subsequent studies in humans. The amino acid sequence in monkey C-peptide differs slightly from that of human in that the fifth amino acid from the N-terminal is proline instead of leucine (Figure 11). However, this difference is small and the differing amino acid is not located in any of the portions of the peptide reported to be important for the biological activity and for cell membrane interactions (124, 129, 149).

Possible influences of the prosthetic group on the observed distribution pattern are not easily characterized since these are the first reported imaging based C-peptide in vivo distribution studies. There is therefore no other data available for comparison. However, the observed distribution of radioactivity, mainly to the kidneys with minor levels in the liver, is consistent with previous information on C-peptide distribution. Furthermore, the few blood samples obtained indicated a plasma half-life of radioactivity slightly larger than 30 min, which is also in agreement with previous findings. Contrary to the reported small amount of intact C-peptide excreted via the urine (131), we here observed a large amount of radioactivity in the urinary bladder. This is presumed to be due to radioactive metabolites and not intact [^{18}F]FB-C-peptide. During the up to 2 h scan, no radioactivity uptake in the skeleton was observed which would have been expected if defluorination had occurred. Other unambiguous statements about the metabolic stability of the radiotracer were not possible though metabolite analysis by gelfiltration of plasma samples was attempted (see discussion below). The fluxes of radioactivity in organs of interest were observed, which enabled radiation dosimetry estimates for subsequent human studies.

Human studies (paper VI)

The distribution studies of [^{18}F]FB-C-peptide in humans (subjects #1-6) were focused on the kidneys since major beneficial effects of C-peptide on renal function in type 1 DM patients have been reported. With the Ecat Exact 31 PET camera, a body segment of only 10 cm could be selected for the dynamic scanning. The scanning protocols used are summarized in Table 4. Subject #1, a healthy volunteer, was screened initially to verify the study protocol which was designed based on the monkey studies. The inclusion of at least one C-peptide producer with the non-producing type 1 DM patients might also provide input for new studies should the imaging reveal major differences in distribution, even though such comparisons can of course only be considered as exploratory. Two of the subjects (#4,5) were administered with carrier non-radioactive C-peptide added (c.a.) in pharmacological dose together with the radiotracer. Further, in one subject (#6) the kinetics of the initial radioactivity distribution was followed in the heart, since it is also positively influenced by C-peptide administration in type 1 DM.

Subject No	Dynamic scan: Segment and time	Static scan: Segment and time	n.c.a or c.a.
1	kidneys, 0-60 min	urinary bladder, 75-85 min; head, 90-105 min	n.c.a.*
2	kidneys, 0-60 min	whole body, from ca. 70 min	n.c.a.
3	kidneys, 0-60 min	whole body, from ca. 70 min	n.c.a.
4	kidneys, 0-60 min		c.a.
5	kidneys, 0-60 min		c.a.
6	heart, 0-75 min		n.c.a.

* healthy volunteer with endogenous C-peptide production

Table 4. Subjects and study protocol for the PET studies performed with [^{18}F]FB-C-peptide in volunteering type 1 DM patients (with or without carrier C-peptide added, c.a. or n.c.a.). All of the subjects were males (mean 30 years) and the DM duration was 16 years (mean) for subjects #2-6.

The PET images showed that, following iv injection of [^{18}F]FB-C-peptide, most of the radioactivity distributed to the kidneys. Visual inspection of coronal images from different time frames, revealed that the radioactivity reached and entered the renal cortex within the first few frames whereafter it gradually was transported to the pelvis and the urethers (Figure 14b). Urinary excretion of radioactivity was also obvious from the scan over the urinary bladder (#1) and from the whole body scans (#2,3) started 70 min after tracer injection and only showing distinct levels of radioactivity in the urinary excretion pathway (including renal pelvis).

Low amounts of radioactivity were detected in the liver. No other organs could be clearly distinguished in the renal scans, although in some subjects, structures resembling

the pancreas and spleen were vaguely discernable. The late scan over the head did not reveal radioactivity in the brain. PET images from the thoracic scan showed a high concentration of radioactivity in the heart and lower in the lungs (Figure 14a).
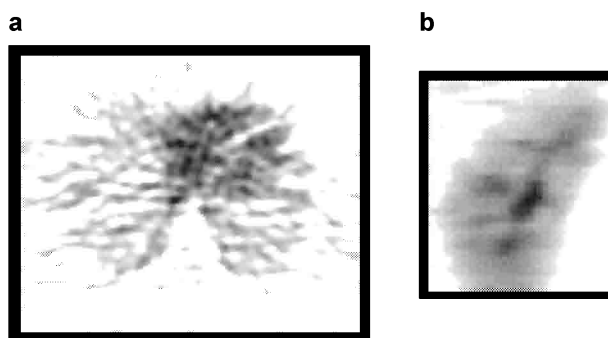

Figure 14. PET images: (a) transaxial plane from the thoracic scan (sum 0-6 min post injection); (b) coronal renal plane showing the renal cortex and radioactivity already in the pelvic area (sum 0-10 min)

Time-radioactivity curves for some organs and for plasma are shown in Figure 15a. The radioactivity distributed rapidly to all of the studied organs. The descending parts of the curves were all best described by functions containing two exponential terms. Based on the similarity in shape and half-lives for the heart and lung curves to those of plasma, the predominant signal from these organs appears to be due to radioactivity in the blood pool. Furthermore, the septum is clearly visible in the PET image indicating much lower levels of radioactivity in the heart muscle than in the blood, even in later time frames when the radioactivity in blood had decreased.

Radioactivity in the area of the erector musculature adjacent to the vertebral column could be distinguished in the late time frames. The time-radioactivity curves from these muscle ROIs were erratic and the concentrations low (around 0.0004-0.0007% id/mL), but these levels were reached within less than 10 min and were essentially maintained throughout the study. Considering the large mass of skeletal muscle in the body (ca 28 kg in man (156)) and assuming the density of muscles to be 1, ca. 15% id was estimated to be localized to the skeletal muscles. This is in good agreement with previously reported estimates, based on arterio-venous differences, that ca. 20% of administered C-peptide is taken up by the resting musculature or retained in the capillary bed (119). However, these PET studies do not reveal whether the radioactivity was in the muscles/myocardium or in the capillaries, nor if it was intact [^{18}F]FB-C-peptide.

Time-radioactivity curves for renal cortex ROIs peaked in the second and third time frame for c.a. (#4,5) and n.c.a. (#2,3) studies, respectively. The subsequent decrease had an alpha half-life of ca. 4 min for all subjects whereas the beta half-life was longer in

the c.a. than in the n.c.a. subjects (ca 45 and 30 min, respectively). Also in the liver, the beta half-life was longer in the c.a. than in the n.c.a. subjects (ca 35 and 23 min, respectively) though peak times and alpha half-lives were the same. Even though the study population is not large enough for the observations to have statistical significance, the longer beta phases for the c.a. studies suggest that the kinetics are affected by the C-peptide concentration. The slightly longer time to reach peak levels in the renal n.c.a. studies may possibly reflect differences in the binding process secondary to differences in the pool size of C-peptide. Differences in estimated urinary excretion of radioactivity also suggest an effect of pool size. For the normal subject (#1) the urine was estimated to account for approximately 15% id at ca. 80 min after the injection, whereas the corresponding value was ca. 55% in two of the type 1 DM subjects (#2,3) receiving n.c.a.. tracer.
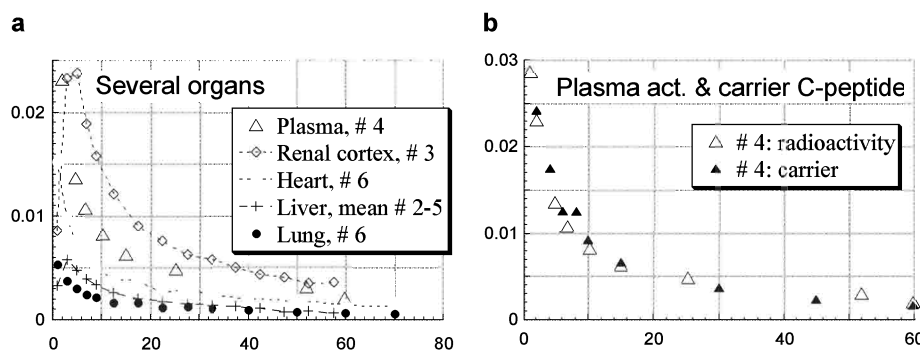

Figure 15. Time-concentration curves with variation in concentration (% id/mL) over time (min): (**a**) radioactivity curves for selected organs and plasma; (**b**) plasma levels of radioactivity and of ELISA-measured concentration of C-peptide.

The reason for the observed differences is not clear to us. Even though the C-peptide plasma half-life is reported to be slightly longer in type 1 DM (131), the metabolic clearance rate of C-peptide is similar in healthy subjects and in type 1 DM patients (131, 134, 157). Further studies are required to elucidate whether these observed tendencies are more than inter-individual variations.

General discussion on the PET studies

The PET protocols (papers V and VI) were not optimized for studying a tracer - receptor interaction. The interaction between C-peptide and a receptor, which has been proposed based on FCS studies with Rh-C-peptide, is saturated at physiological C-peptide concentrations (0.9 nM) and binding of Rh-C-peptide is blocked to 50% at even lower (0.3 nM) C-peptide levels (129). A report of specific binding of tyrosinated ^{125}I-labeled C-peptide analog in vitro to a rat islet tumor cell line indicated a low and a high

affinity component with 440 and 4880 binding sites per cell, respectively (158). However, specific binding of radioanalogs of C-peptide have, to the best of our knowledge, not been reported elsewhere even though attempts have been made, e.g. with membranes from skeletal muscles (159).

The s.r. of the [^{18}F]FB-C-peptide used in the performed PET studies, resulted in a FB-C-peptide content of ca. 0.5-2.8 nmole in the dose administered in the n.c.a. experiments. Evenly distributed in the blood pool (assumed ca. 4.5 l) the resulting concentration of ca. 0.1-0.6 nM, would be sufficiently high to at least partially block radiotracer - receptor interaction. The n.c.a. studies are thus not carrier-free, which should be kept in mind when making a comparison with the studies with c.a. pharmacological doses. For one of the c.a. subjects (#4), C-peptide in plasma was followed over time by ELISA analysis. Plasma radioactivity and the ELISA measured C-peptide concentrations were very similar, as shown in Figure 15b. Since the plasma time-radioactivity curves for all the subjects were very similar, it appears that [^{18}F]FB-C-peptide is extracted from the plasma pool similarly to native C-peptide in n.c.a. as well as c.a. conditions.

Attempts were made to examine for low molecular radioactive metabolites in plasma using gel filtration chromatography and on HPLC analysis of ultra-filtrate. In the former, though essentially all radioactivity eluted in the high molecular fraction, it can not be excluded that N-terminal labeled C-peptide fragments also co-eluted. The HPLC analysis was, unfortunately, inconclusive since the counting statistics were too low. The PET images showed no evidence of defluorination since radioactivity in the bones was not detected. There is a possibility that the prosthetic group-peptide linkage (139) as well as the peptide itself can be cleaved. However, radioactivity and ELISA based plasma peptide estimations (Figure 15b) showed, if not direct information about the in vivo stability of [^{18}F]FB-C-peptide, at least that the radioactivity and immunoreactive C-peptide in plasma are similarly extracted. It can not be excluded that ELISA also detects fragments of C-peptide. However, the ELISA kit used (Mercodia, Uppsala, Sweden) is marketed as measuring intact C-peptide through interactions of two MAbs that are directed against separate antigenic determinants located at each end of the C-peptide chain. Theoretically, only C-peptide molecules with intact N- and C-terminal should be detected. Unfortunately, no data is available concerning whether cross reaction can occur with C-peptide fragments lacking only a few amino acid residues in either or both ends.

The C-peptide distribution and kinetic data obtained from the performed PET studies are affected by limitations inherent to the use of [^{18}F]FB-C-peptide. This labeled tracer permits only the detection of peptide fragments that retain the N-terminal. Accumulated studies suggest that fragments of C-peptide may contribute to the biological action (see discussion above). Labeled peptide fragments lacking the C-terminal have been detected

in plasma after 2 hours infusion of ^{125}I-tyrosylated (N-terminally) human C-peptide in monkey (160). To obtain further knowledge on the distribution of C-peptide and fragments, other radiolabels should be incorporated in different positions and/or in different fragments of the peptide. Performing such studies in animal models would permit metabolite analysis not only of blood samples, but also of organ extracts or homogenates to identify the fragments present at the proposed sites of action.

Despite all the information we have yet to obtain, the performed PET studies constitute the first imaging-based in vivo distribution studies reported for C-peptide. Besides the larger and smaller distribution to the kidneys and liver, respectively, predicted by previous findings, radioactivity localized in regions corresponding to skeletal muscle, but not in the brain or, to a large extent, in any other region within the parts of the trunk scanned. Furthermore, organ specific kinetics for concentration variations of the radioactivity has been described. Renal kinetics were fast, while concentrations in the muscle area were fairly constant over the hour scanned. Additional information on C-peptide's in vivo behavior is warranted in light of its potential for treating (amelioration or postponed onset) long-term complications of type 1 DM, whose worldwide incidence is estimated to increase by about 40% between 1998 and 2010 (161).

SUMMARY OF FINDINGS AND CONCLUSIONS

^{11}C-Labeled PD153035

♦ Methods to synthesize desmethyl-PD153035 compounds have been developed. Both the two mono-demethylated constitutional isomers and the di-demethylated compound were obtained. Thus different positions for the labeling can be chosen for performing in vivo metabolite studies.

♦ Radiolabeling conditions have been found by which the radiotracer [6-methoxy-^{11}C]PD153035 can be produced from [^{11}C]methyl iodide in yields and quality suitable for the intended PET studies.

♦ The strategy for cleaving methyl phenyl ethers using methanesulfonic acid and microwave-induced heating may find broader application in PET radiochemistry for rapidly obtaining other desmethyl precursors and for post-labeling removal of methyl protective groups.

♦ The distribution of [6-methoxy-^{11}C]PD153035 over time to different organs has been examined in vivo in rat using PET. The rapid kinetics observed are well suited for the half-life of radionuclide used.

♦ PET distribution studies to proliferating tissue in rats with a xenografted tumor model revealed levels of radioactivity in the tumor sites that appeared to correlate to tumor viability, determined postmortem.

♦ The encouraging initial screening studies suggest that the potential of carbon-11 labeled PD153035 to non-invasively assess EGFR level warrants further evaluation.

^{18}F-Labeled fluorobenzoyl-C-peptide ([^{18}F]FB-C-peptide)

♦ A method for labeling the relatively small and hydrophilic C-peptide with a positron-emitting radionuclide has been developed, based on the fluorine-18 labeled prosthetic group N-succinimidyl-4-[^{18}F]fluorobenzoate. C-peptide which was ^{18}F-labeled in the N-terminal could be obtained in yields sufficient for the planned PET investigations.

♦ PET studies of [^{18}F]FB-C-peptide in monkey identified the kidneys as the major target organ and revealed distribution of radioactivity to the kidneys and heart, small amounts to the liver and lungs, as well as urinary excretion. The kinetics in all the studied organs was relatively rapid after bolus iv administration.

♦ Radioactivity distribution in volunteering type 1 DM subjects followed the same pattern. Furthermore, small levels of radioactivity in skeletal muscle could, due to the large total muscle content, account for ca. 15% of the administered dose. A

tendency to altered kinetics, possibly secondary to differences in C-peptide load, was observed in the metabolic organs when carrier C-peptide was added, i.e. time to peak in kidneys, renal and hepatic beta phase half-life and amount of urinary secreted radioactivity.

◆ The observations in the monkey and human PET studies describe the behavior of intact [^{18}F]FB-C-peptide as well as possible fragments retaining the labeled N-terminal. These studies constitute the first imaging-based in vivo distribution studies of labeled C-peptide. The information gained on organ specific kinetics adds to the growing knowledge about C-peptide's in vivo behavior.

ACKNOWLEDGEMENTS

I wish to express my sincere gratitude to all of you who have been around and helped me in various ways during the years when this work has been performed. There are a number of persons that I want to address specifically:

My supervisor Prof. Sharon Stone-Elander for her enthusiasm and knowledge, for introducing me to the fascinating PET field and for making me see the enchantment with this multi-disciplinary research area. I want to thank both Sharon and Nils for their friendship and all the laughter.

My co-supervisor Prof. John Wahren and his colleagues Bo-Lennart Johansson and Karin Ekberg at the Section of Clinical Physiology for the collaboration in the C-peptide project. My special appreciation to Karin for never ending support and for pedagogical discussions on the biological and physiological aspects of C-peptide.

Prof. Martin Ingvar at the Section of Clinical Neurophysiology for collaboration in the PET studies. I also want to thank Martin and the members of the clinical neurophysiology group and PET basic service organization over the years: Elle, Gustav, Johan, Julio, Predrag, Katrina, Jens, Karl-Magnus and Christian for support with PET-data handling and evaluation as well as solving computer problems and for being easy to get along with.

Dr Jan-Olov Thorell and Dr Peter Johnström for initial guidance in the PET chemistry field, collaboration and friendship.

Everybody at the Karolinska Pharmacy, with special thanks to Prof. Hans Ehrsson, Assoc. Prof. Staffan Eksborg and farmacist Inger Wallin; also the present and former staff at "Forskningen" including Annika, Birgitta, Carina, Elin, Gareth, Helen, Maria, Pernilla, Vahid and Walter; as well as Birgit Garmelius and Kjell Rudeaus from the production unit.

Co-authors, Moustapha Hassan, Per Kogner, Per Borgström, Per Jonasson, Per-Åke Nygren for their contributions to these research projects.

Prof. Christer Halldin and the former and present members of the Psychiatry radiochemistry group: Johan and Camilla, Jari, Magnus, Phong and Arsalan for pleasant and enjoyable company and interactions both in and outside the PET lab - including the ethanol production ☺.

Göran Printz, Peter Söderholm, Dennis Eriksson and Christer Dupuis for the radionuclide productions and cyclotron attendance.

Hans Jacobsson, Stig Larsson, Per-Olof Schnell and Cathrine Jonsson at Nuclear Medicine for sharing their knowledge in fruitful discussions.

All my friends!! Especially Anna and Marie for all chats and enjoyment. Harriet for deep and valuable friendship.

My father Lars and brother Niclas and Christer, my small sisters Karin and Astrid, Susanne and her family for love, encouragement and for never doubting my success with the "impossible".

Anita, my aunt, who is a wonderful and warm person with inexhaustible love and solicitude to whom I owe my fullest affection and esteem. Likewise, I want to thank my uncle Stig and all my cousins.

The Ellburg family: Ulla and Christer, Marika and her family, for amicability and a lot of fun.

Last, but most importantly, Mårten the light in my life, for support, care and love.

REFERENCES

1. Ter-Pogossian MM. (1995) Positron emission tomography (PET). In: *Principles of nuclear medicine*. pp. 342-377; Edited by Wagner Jr. HN, Szabo Z and Buchanan JW. W.B. Saunders Company, London.

2. Meikle SR and Dahlbom M. (1994) Positron emission tomography. In: *Nuclear medicine in clinical diagnosis and treatment*. pp. 1327-1337; Edited by Murray IPC and Ell PJ. Churchill Livingstone, London.

3. Jones T. (1996) The imaging science of positron emission tomography. *Eur. J. Nucl. Med.* **23**, 807-813.

4. Jaszczak RJ and Tsui BMW. (1995) Single photon emission computed tomography (SPECT). In: *Principles of nuclear medicine*. pp. 317-341; Edited by Wagner Jr. HN, Szabo Z and Buchanan JW. W.B. Saunders Company, London.

5. Bailey DL and Parker JA. (1994) Single photon emission computerized tomography. In: *Nuclear medicine in clinical diagnosis and treatment*. pp. 1315-1326; Edited by Murray IPC and Ell PJ. Churchill Livingstone, London.

6. Croft BY. (1990) Instrumentation and computers for brain single photon emission computed tomography. *Semin. Nucl. Med.* **20**, 281-289.

7. Phelps ME. (2000) PET: the merging of biology and imaging into molecular imaging. *J. Nucl. Med.* **41**, 661-681.

8. Saleem A, Aboagye EO and Price PM. (2000) In vivo monitoring of drugs using radiotracer techniques. *Adv. Drug Deliv. Rev.* **41**, 21-39.

9. Brady F, Luthra SK, Brown GD, Osman S, Aboagye E, Saleem A and Price PM. (2001) Radiolabelled tracers and anticancer drugs for assessment of therapeutic efficacy using PET. *Curr. Pharm. Des.* **7**, 1863-1892.

10. Price P. (2001) PET as a potential tool for imaging molecular mechanisms of oncology in man. *Trends Molec. Med.* **7**, 442-446.

11. Pilowsky LS. (2001) Probing targets for antipsychotic drug action with PET and SPET receptor imaging. *Nucl. Med. Comun.* **22**, 829-833.

12. Workman P. (1995) Bottlenecks in anticancer drug discovery and development: in vivo pharmacokinetic and pharmacodynamic issues and the potential role of PET. In: *PET for drug development and evaluation*. pp. 277-285; Edited by Comar D. Kluwer Academic Publishers, London.

13. Farde L. (1996) The advantage of using positron emission tomography in drug research. *Trends. Neurosci.* **19**, 211-214.

14. Fowler JS, Volkow ND, Wang G-J, Ding Y-S and Dewey SL. (1999) PET and drug research and development. *J. Nucl. Med.* **40**, 1154-1163.

15. Gibson RE, Burns HD, Hamill TG, Eng W-S, Francis BE and Ryan C. (2000) Non-invasive radiotracer imaging as a tool for drug development. *Curr. Pharm. Des.* **6**, 973-989.

16. Aboagye EO, Price PM and Jones T. (2001) In vivo pharmacokinetics and pharmacodynamics in drug development using positron-emission tomography. *Drug Discov. Today* **6**, 293-302.

17. Cherry SR. (2001) Fundamentals of positron emission tomography and applications in preclinical drug development. *J. Clin. Pharmacol.* **41**, 482-491.

18. Ter-Pogossian MM and Wagner Jr. HN, (1998) A new look at the cyclotron for making short-lived isotopes. 1966 -classical article. *Semin. Nucl. Med.* **28**, 202-212.

19. McCarthy TJ and Welch MJ. (1998) The state of positron emitting radionuclide production in 1997. *Semin. Nucl. Med.* **28**, 235-246.

20. Budinger TF. (1998) PET instrumentation: what are the limits? *Semin. Nucl. Med.* **28**, 247-267.

21. Mazière B, Cantineau R, Coenen HH, Guillaume M, Halldin C, Luxen A, Loc'h C and Luthra SK. (1993) PET radiopharmaceutical metabolism - plasma metabolite analysis. In: *Radiopharmaceuticals for positron emission tomography.* pp. 151-178; Edited by Stöcklin G and Pike VW. Kluwer Academic Publishers, London.

22. Mazoyer B. (1995) Positron emission tomography: Basic principles and potential interest for pharmacological studies. In: *PET for drug development and evaluation.* pp. 25-35; Edited by Comar D. Kluwer Academic Publishers, London.

23. Långström B, Bergström M, Hartvig P, Valind S and Watanabe Y. (1995) Is PET a tool for drug evaluation?. In: *PET for drug development and evaluation.* pp. 37-50; Edited by Comar D. Kluwer Academic Publishers, London.

24. Långström B and Dannals RF. (1995) Radiotracer production: Carbon-11 compounds. In: *Principles of nuclear medicine.* pp. 166-178; Edited by Wagner Jr. HN, Szabo Z and Buchanan JW. W.B. Saunders Company, London.

25. Stöcklin G. (1995) Radiotracer production: Fluorine-18 compounds. In: *Principles of nuclear medicine.* pp. 178-194; Edited by Wagner Jr. HN, Szabo Z and Buchanan JW. W.B. Saunders Company, London.

26. Björkman M, Doi H, Resul B, Suzuki M, Noyori R, Watanabe Y and Långström B. (2000) Synthesis of a ^{11}C-labelled prostaglandin F2α analogue using an improved method for Stille reactions with [^{11}C]methyl iodide. *J. Labelled Cpd. Radiopharm.* **43**, 1327-1334.

27. Bergman J and Solin O. (1997) Fluorine-18-labeled fluorine gas for sythesis of tracer moelcules. *Nucl. Med. Biol.* **24**, 677-683.

28. Tsui BMW, Zhao X, Frey EC and McCartney WH. (1994) Quantitative single-photon emission computed tomography: basics and clinical considerations. *Semin. Nucl. Med.* **24**, 38-65.

29. Raymond E, Faivre S and Armand JP. (2000) Epidermal growth factor receptor tyrosine kinase as a target for anticancer therapy. *Drugs* **60**, 15-23.

30. Yarden Y and Schlessinger J. (1987) Self-phosphorylation of epidermal growth factor receptor: evidence for a model of intermolecular allosteric activation. *Biochemistry* **26**, 1434-1442.

31. Cohen S, Ushiro H, Stoscheck C and Chinkers M. (1982) A native 170,000 epidermal growth factor receptor-kinase complex from shed plasma membrane vesicles. *J. Biol. Chem.* **257**, 1523-1531.

32. Iwashita S and Kobayashi M. (1992) Signal transduction system for growth factor receptors associated with tyrosine kinase activity: epidermal growth factor receptor signalling and its regulation. *Cell. Signal.* **4**, 123-132.

33. Plata-Salamán CR. (1991) Epidermal growth factor and the nervous system. *Peptides* **12**, 653-663.

34. Salomon DS, Brandt R, Ciardiello F and Normanno N. (1995) Epidermal growth factor-related peptides and their receptors in human malignancies. *Crit. Rev. Oncol./Hematol.* **19**, 183-232.

35. Gullick WJ. (1991) Prevalence of aberrant expression of the epidermal growth factor receptor in human cancers. *Br. Med. Bull.* **47**, 87-98.

36. Eccles SA, Modjtahedi H, Box G, Court W, Sandle J and Dean CJ. (1994-95) Significance of the c-erbB family of receptor tyrosine kinases in metastatic cancer and their potential as targets for immunotherapy. *Invasion Metastasis* **14**, 337-348.

37. Seymour LK. (2001) Epidermal growth factor receptor as a target: recent developments in the search for effective new anti-cancer agents. *Curr. Drug Targets* **2**, 117-133.

38. Woodburn JR. (1999) The epidermal growth factor receptor and its inhibition in cancer therapy. *Pharmacol. Ther.* **82**, 241-250.

39. Siegall CB. (1994) Targeted toxins as anticancer agents. *Cancer* **74**, 1006-1012.

40. Reist CJ, Foulon CF, Alston K, Bigner DD and Zalutsky MR. (1999) Astatine-211 labeling of internalizing anti-EGFRvIII monoclonal antibody using N-succinimidyl 5-[^{211}At]astato-3-pyridinecarboxylate. *Nucl. Med. Biol.* **26**, 405-411.

41. Carlsson J, Gedda L, Grönvik C, Hartman T, Lindström A, Lindström P, Lundqvist H, Lövqvist A, Malmqvist J, Olsson P, Essand M, Pontén J, Sjöberg S and Westermark B. (1994) Strategy for boron neutron capture therapy against tumor cells with over-expression of the epidermal growth factor-receptor. *Int. J. Radiat. Oncol. Biol. Phys.* **30**, 105-115.

42. Davies DE and Chamberlin SG. (1996) Targeting the epidermal growth factor receptor for therapy of carcinomas. *Biochem. Pharmacol.* **51**, 1101-1110.

43. Ciardiello F. (2000) Epidermal growth factor receptor tyrosine kinase inhibitors as anticancer agents. *Drugs* **60**, 25-32.

44. Strauss LG and Conti PS. (1991) The applications of PET in clinical oncology. *J. Nucl. Med.* **32**, 623-648 (discussion 649-650).

45. Pauwels EKJ, McCready VR, Stoot JHMB and van Deurzen DFP. (1998) The mechanism of accumulation of tumour-localising radiopharmaceuticals. *Eur. J. Nucl. Med.* **25**, 277-305.

46. Katzenellenbogen JA, Coleman RE, Hawkins RA, Krohn KA, Larson SM, Mendelsohn J, Osborne CK, Piwnica-Worms D, Reba RC, Siegel BA, Welch MJ and Shtern F. (1995) Tumor receptor imaging: proceedings of the National Cancer Institute workshop, review of current work, and prospective for further investigations. *Clin. Cancer Res.* **1**, 921-932.

47. Escobar NI, Morales AM, Ducongé J, Torres IC, Fernández E and Gómez JA. (1998) Pharmacokinetics, biodistribution and dosimetry of ^{99m}Tc-labeled anti-human epidermal growth factor receptor humanized monoclonal antibody R3 in rats. *Nucl. Med. Biol.* **25**, 17-23.

48. Orlova A, Bruskin A, Sjöstrom A, Lundqvist H, Gedda L and Tolmachev V. (2000) Cellular processing of [^{125}]I- and [^{111}]In-labeled epidermal growth factor (EGF) bound to cultured A431 tumor cells. *Nucl. Med. Biol.* **27**, 827-835.

49. Wen X, Wu Q-P, Ke S, Ellis L, Charnsangavej C, Delpassand AS, Wallace S and Li C. (2001) Conjugation with [^{111}]In-DTPA-poly(ethylene glycol) improves imaging of anti-EGF receptor antibody C225. *J. Nucl. Med.* **42**, 1530-1537.

50. Bishop PC, Myers T, Robey R, Fry DW, Liu ET, Blagosklonny MV and Bates SE. (2002) Differential sensitivity of cancer cells to inhibitors of the epidermal growth factor receptor family. *Oncogene* **21**, 119-127.

51. Ramos-Suzarte M, Rodriguez N, Oliva JP, Iznaga-Escobar N, Perera A, Morales A, Gonzales N, Cordero M, Torres L, Pimentel G, Borrón M, González J, Torres O, Rodriguez T and Pérez R. (1999) ^{99m}Tc-Labeled antihuman epidermal growth factor receptor antibody in patients with tumors of epithelial origin: Part III. clinical trials safety and diagnostic efficacy. *J. Nucl. Med.* **40**, 768-775.

52. Zalutsky MR, Xu FJ, Yu Y, Foulon CF, Zhao X-G, Slade SK, Affleck DJ and Bast Jr. RC. (1999) Radioiodinated antibody targeting of the HER-2/neu oncoprotein: Effects of labeling method on cellular processing and tissue distribution. *Nucl. Med. Biol.* **26**, 781-790.

53. Zhao Q, Tolmachev V, Carlsson J, Lundqvist H, Sundin J, Janson J-C and Sundin A. (1999) Effects of dextranation on the pharmacokinetics of short peptides. A PET study on mEGF. *Bioconjugate Chem.* **10**, 938-946.

54. Workman P, Brunton VG and Robins DJ. (1992) Tyrosine kinase inhibitors. *Semin. Cancer Biol.* **3**, 369-381.

55. Levitzki A. (1999) Protein tyrosine kinase inhibitors as novel therapeutic agents. *Pharmacol. Ther.* **82**, 231-239.

56. Elder JT, Fisher GJ, Lindquist PB, Bennett GL, Pittelkow MR, Coffey Jr. RJ, Ellingsworth L, Derynck R and Voorhees JJ. (1989) Overexpression of transforming growth factor alpha in psoriatic epidermis. *Science* **243**, 811-814.

57. Levitzki A. (1992) Tyrphostins: tyrosine kinase blockers as novel antiproliferative agents and dissectors of signal transduction. *FASEB J* **6**, 3275-3282.

58. Levitzki A and Gazit A. (1995) Tyrosine kinase inhibition: an approach to drug development. *Science* **267**, 1782-1788.

59. Lawrence DS and Niu J. (1998) Protein kinase inhibitors: the tyrosine-specific protein kinases. *Pharmacol. Ther.* **77**, 81-114.

60. Fry DW. (1996) Recent advances in tyrosine kinase inhibitors. *Ann. Rep. Med. Chem.* **31**, 151-160.

61. Traxler P and Furet P. (1999) Strategies toward the design of novel and selective protein tyrosine kinase inhibitors. *Pharmacol. Ther.* **82**, 195-206.

62. Bos M, Mendelsohn J, Kim Y-M, Albanell J, Fry DW and Baselga J. (1997) PD153035, a tyrosine kinase inhibitor, prevents epidermal growth factor receptor activation and inhibits growth of cancer cells in a receptor number-dependent manner. *Clin. Cancer Res.* **3**, 2099-2106.

63. Faust RA, Tawfic S, Davis AT and Ahmed K. (1999) Apoptosis and growth inhibition of head and neck tumor cell line induced by epidermal growth factor receptor tyrosine kinase inhibitor. *Oral Oncol.* **35**, 290-295.

64. Powell TJ, Ben-Bassat H, Klein BY, Chen H, Shenoy N, McCollough J, Narog B, Gazit A, Harzstark Z, Chaouat M, Levitzki R, Tang C, McMahon J, Shawver L and Levitzki A. (1999) Growth inhibition of psoriatic keratinocytes by quinazoline tyrosine kinase inhibitors. *Br. J. Dermatol.* **141**, 802-810.

65. Fry DW, Kraker AJ, McMichael A, Ambroso LA, Nelson JM, Leopold WR, Connors RW and Bridges AJ. (1994) A specific inhibitor of the epidermal growth factor receptor tyrosine kinase. *Science* **265**, 1093-1095.

66. Mulholland GK, Winkle W, Mock BH and Sledge G. (1995) Radioiodinated epidermal growth factor receptor ligands as tumor probes. Dramatic potentiation of binding to MDA-468 cancer cells in presence of EGF. *J. Nucl. Med.* **36**, P71.

67. Lim JK, Negash K, Hanrahan SM and VanBrocklin HF. (2000) Synthesis of 4-(3'-[^{125}I]iodoanilino)-6,7-dialkoxyquinazolines: radiolabeled epidermal growth factor receptor tyrosine kinase inhibitors. *J. Labelled Cpd. Radiopharm.* **43**, 1183-1191.

68. Mulholland GK, Zheng Q-H, Winkle WL and Carlson KA. (1997) Synthesis and biodistribution of new C-11 and F-18 labeled epidermal growth factor receptor ligands. *J. Nucl. Med.* **38**, P141.

69. Johnström P, Fredriksson A, Thorell J-O, Hassan M, Kogner P, Borgström P, Ingvar M and Stone-Elander S. (1997) Synthesis and in vivo biodistribution of tyrosine kinase inhibitor, [methoxy-^{11}C]PD 153035. *J. Labelled. Cpd. Radiopharm.* **40**, S377-S379.

70. Lim JK, Riese II DJ, Negash K, Hawkins RA and VanBrocklin HF. (1998) Synthesis and *in vitro* evaluation of epidermal growth factor receptor tyrosine kinase inhibitors. *J. Nucl. Med.* **39**, P20.

71. Lim JK, Riese II DJ and VanBrocklin HF. (1999) Synthesis of 4-(4'-[^{18}F]fluorobenzylamino)-6,7-diethoxyquinazoline: a positron emitting radioprobe for the epidermal growth factor receptor. *J. Labelled Cpd. Radiopharm.* **42**, S693-S695.

72. Mishani E, Bonasera TA, Rozen Y, Ortu G, Gazit A and Levitzki A. (1999) Fluorinated EGFR-TK inhibitor-based tracers for PET. *J. Labelled Cpd. Radiopharm.* **42**, S27-S29.

73. Bonasera TA, Ortu G, Rozen Y, Krais R, Freedman NMT, Chisin R, Gazit A, Levitzki A and Mishani E. (2001) Potential ^{18}F-labeled biomarkers for epidermal growth factor receptor tyrosine kinase. *Nucl. Med. Biol.* **28**, 359-74.

74. Snyder SE, Whitmer KM and Brown-Proctor C. (1999) Synthesis of 3-chloro-4-[^{18}F]fluoroaniline as a synthon for epidermal growth factor receptor inhibitors for tumor imaging with PET. *J. Labelled Cpd. Radiopharm.* **42**, S522-S524.

75. Snyder SE, Sherman PS and Blair JB. (2000) 4-(3-Chloro-4-[^{18}F]fluorophenylamino)-6,7-dimethoxyquinazoline: a radiolabeled EGF receptor inhibitor for imaging tumor biochemistry with PET. *J. Nucl. Med.* **41**, 233P.

76. Mishani E, Ben-David I, Rozen Y, Ortu G and Levitzki A. (2001) Carbon-11 labeled irreversible inhibitors for mapping epidermal growth factor receptor tyrosine kinase (EGFR-TK). *J. Labelled Cpd. Radiopharm.* **44**, S99-S101.

77. Ortu G, Ben-David I, Rozen Y, Levitzki A and Mishani E. (2001) Biological evaluation of a novel ^{11}C labelled irreversible EGFRTK inhibitor. *Q. J. Nucl. Med.* **45**, S7.

78. Bolton R. (2001) Isotopic methylation. *J. Labelled Cpd. Radiopharm.* **44**, 701-736.

79. Rewcastle GW, Denny WA, Bridges AJ, Zhou H, Cody DR, McMichael A and Fry DW. (1995) Tyrosine kinase inhibitors. 5. Synthesis and structure-activity relationships for 4-[(phenylmethyl)amino]- and 4-(phenylamino)quinazolines as potent adenosine 5'-triphosphate binding site inhibitors of the tyrosine kinase domain of the epidermal growth factor receptor. *J. Med. Chem.* **38**, 3482-3487.

80. Bhatt MV and Kulkarni SU. (1983) Cleavage of ethers. *Synthesis* **4**, 249-282.

81. Abramovitch RA. (1991) Applications of microwave energy in organic chemistry. A review. *Org. Prep. Proced. Int.* **23**, 683-711.

82. Caddick S. (1995) Microwave assisted organic reactions. *Tetrahedron* **51**, 10403-10432.

83. Lidström P, Tierney J, Wathey B and Westman J. (2001) Microwave assisted organic synthesis - a review. *Tetrahedron* **57**, 9225-9283.

84. Elander N, Jones JR, Lu S-Y and Stone-Elander S. (2000) Microwave-enhanced radiochemistry. *Chem. Soc. Rev.* **29**, 239-249.

85. Stone-Elander S and Elander N. (2002) Microwave applications in radiolabelling with short-lived positron-emitting radionuclides. *J. Labelled Cpd. Radiopharm.*, in press.

86. Kulkarni PP, Kadam AJ, Mane RB, Desai UV and Wadgaonkar PP. (1999) Demethylation of methyl aryl ethers using pyridine hydrochloride in solvent-free conditions under microwave irradiation. *J. Chem. Research. (S)* **6**, 394-395.

87. Oussaïd A, Thach LN and Loupy A. (1997) Selective dealkylations of alkyl aryl ethers in heterogenous basic media under microwave irradiation. *Tetrahedron Lett.* **38**, 2451-2454.

88. Stone-Elander S, Fredriksson A and Elander N. (2001) Strategies for rapid deprotections: a screening study on methyl phenyl ether. *J. Labelled Cpd. Radiopharm.* **44**, S1029-S1031.

89. Fujii N, Irie H and Yajima H. (1977) Regioselective cleavage of aromatic methyl ethers by methanesulphonic acid in the presence of methionine. *J. Chem. Soc. Perkin Trans. I* 2288-2289.

90. Gibson KH. (1998) Quinazoline derivatives. Zeneca Limited (London, GB), *US patent & trademark office, Patent full text and image database*; US.

91. Luxen A, Guillaume M, Melega WP, Pike VW, Solin O and Wagner R. (1992) Production of 6-[^{18}F]fluoro-L-dopa and its metabolism in vivo - a critical review. *Nucl. Med. Biol.* **19**, 149-158.

92. Ehrin E, Johnström P, Stone-Elander S, Nilsson JLG, Persson A, Farde L, Sedvall G, Litton J-E, Eriksson L, Widén L and Greitz T. (1984) Preparation and preliminary positron emission tomography studies of ^{11}C-Ro 15-1788, a selective benzodiazepine receptor antagonist. *Acta Pharm. Suec.* **21**, 183-188.

93. Farde L, Halldin C, Stone-Elander S and Sedvall G. (1987) PET analysis of human dopamine receptor subtypes using ^{11}C-SCH 23390 and ^{11}C-raclopride. *Psychopharmacology* **92**, 278-284.

94. Sandell J, Langer O, Larsen P, Dolle F, Vaufrey F, Demphel S, Crouzel C and Halldin C. (2000) Improved specific radioactivity of the PET radioligand [^{11}C]FLB 457 by use of the GE Medical Systems PETtrace MeI MicroLab. *J. Labelled Cpd. Radiopharm.* **43**, 331-338.

95. Larsen P, Ulin J, Dahlström D and Jensen M. (1997) Synthesis of [^{11}C]iodomethane by iodination of [^{11}C]methane. *Appl. Radiat. Isot.* **48**, 153-157.

96. Lundkvist C, Sandell J, Någren K, Pike VW and Halldin C. (1998) Improved syntheses of the PET radioligands, [^{11}C]FLB 457, [^{11}C]MDL 100907 and [^{11}C]β-CIT-FE, by the use of [^{11}C]methyl triflate. *J. Labelled Cpd. Radiopharm.* **41**, 545-556.

97. Meyers MB, Shen WPV, Spengler BA, Ciccarone V, O'Brien JP, Donner DB, Furth ME and Biedler JL. (1988) Increased epidermal growth factor receptor in multidrug-resistant human neuroblastoma cells. *J. Cell. Biochem.* **38**, 87-97.

98. Kunkel MW, Hook KE, Howard CT, Przybranowski S, Roberts BJ, Elliott WL and Leopold WR. (1996) Inhibition of the epidermal growth factor receptor tyrosine kinase by PD153035 in human A431 tumors in athymic nude mice. *Invest. New Drugs* **13**, 295-302.

99. Mattner F, Katsifis A, Dikic B, Greguric I, Chapman J and Papazian V. (2001) Radioiodinated epidermal growth factor receptor inhibitors for tumor imaging with SPECT. *Q. J. Nucl. Med.* **45**, S6.

100. Das M, Rengaraju M and Samanta A. (1992) Epidermal growth factor. In: *Human Cytokines: Handbook for basic and clinical research.* pp. 365-373; Edited by Aggarwal BB and Gutterman JU. Blackwell Scientific Publications, Boston.

101. Jacquemin-Sablon A, Agbotounou WK and Pierre J. (1995) Les inhibiteurs de protéine-tyrosine kinases: Perspectives pharmacologiques? *Pathol. Biol. (Paris)* **43**, editorial, 389-394.

102. Eckelman WC. (1994) The application of receptor theory to receptor-binding and enzyme-binding oncologic radiopharmaceuticals. *Nucl. Med. Biol.* **21**, 759-769.

103. Smaill JB, Rewcastle GW, Loo JA, Greis KD, Chan OH, Reyner EL, Lipka E, Showalter HDH, Vincent PW, Elliott WL and Denny WA. (2000) Tyrosine kinase inhibitors. 17. Irreversible inhibitors of the epidermal growth factor receptor: 4-(phenylamino)-quinazoline- and 4-(phenylamino)pyrido[3,2-*d*]pyrimidine-6-acrylamides bearing additional solubilizing functions. *J. Med. Chem.* **43**, 1380-1397.

104. Tillhammar P. (1999) Okänt hormon blir läkemedel mot diabetes. *Medicinsk Vetenskap* **1**, 9-12.

105. Andersson D and Berne C. (2001) Diabetes mellitus. In: *Läkemedelsboken 2001/2002.* pp. 471-491; Edited by Bogentoft S. Apoteket AB, Farmaci/Marknad, Stockholm, Sweden.

106. Ziegler D. (2001) New drugs to prevent or treat diabetic polyneuropathy. *Int. Diabetes Monit.* **13**, 1-10.

107. King GL and Brownlee M. (1996) The cellular and molecular mechanisms of diabetic complications. *Endocrinol. Metab. Clin. North Am.* **25**, 255-270.

108. Atkinson MA and Eisenbarth GS. (2001) Type 1 diabetes: new perspectives on disease pathogenesis and treatment. *Lancet* **358**, 221-229.

109. Whelan J. (2000) Reversing age-related and diabetic cardiovascular disease. *Drug Discov. Today* **5**, 272-273.

110. Steiner DF and Oyer PE. (1967) The biosynthesis of insulin and a probable precursor of insulin by a human islet cell adenoma. *Proc. Natl. Acad. Sci. USA* **57**, 473-481.

111. Wahren J, Johansson B-L, Wallberg-Henriksson H, Linde B, Fernqvist-Forbes E and Zierath JR. (1996) C-peptide revisited - new physiological effects and therapeutic implications. *J. Intern. Med.* **240**, 115-124.

112. Kunt T, Forst T, Pfützner A, Beyer J and Wahren J. (1999) The physiological impact of proinsulin C-peptide. *Pathophysiology* **5**, 257-262.

113. Wahren J, Ekberg K, Johansson J, Henriksson M, Pramanik A, Johansson B-L, Rigler R and Jörnvall H. (2000) Role of C-peptide in human physiology. *Am. J. Physiol. Endocrinol. Metab.* **278**, E759-E768.

114. Johansson B-L, Sjöberg S and Wahren J. (1992) The influence of human C-peptide on renal function and glucose utilization in type 1 (insulin-dependent) diabetic patients. *Diabetologia* **35**, 121-128.

115. Johansson B-L, Kernell A, Sjöberg S and Wahren J. (1993) Influence of combined C-peptide and insulin administration on renal function and metabolic control in diabetes type 1. *J. Clin. Endocrinol. Metab.* **77**, 976-981.

116. Johansson B-L, Borg K, Fernqvist-Forbes E, Kernell A, Odergren T and Wahren J. (2000) Beneficial effects of C-peptide on incipient nephropathy and neuropathy in patients with Type 1 diabetes mellitus. *Diabet. Med.* **17**, 181-189.

117. Ekberg K, Brismar T, Lindström P, Johansson B-L and Wahren J. (2002) C-peptide improves sensory nerve function in patients with type 1 diabetes. *American Diabetes Association 62nd Scientific Sessions* June, in press.

118. Johansson B-L, Borg K, Fernqvist-Forbes E, Odergren T, Remahl S and Wahren J. (1996) C-peptide improves autonomic nerve function in IDDM patients. *Diabetologia* **39**, 687-695.

119. Johansson BL, Linde B and Wahren J. (1992) Effects of C-peptide on blood flow, capillary diffusion capacity and glucose utilization in the exercising forearm of type 1 (insulin-dependent) diabetic patients. *Diabetologia* **35**, 1151-1158.

120. Forst T, Kunt T, Pohlmann T, Goitom K, Engelbach M, Beyer J and Pfutzner A. (1998) Biological activity of C-peptide on the skin microcirculation in patients with insulin-dependent diabetes mellitus. *J. Clin. Invest.* **101**, 2036-2041.

121. Johansson B-L, Sundell J, Ekberg K, Jonsson C, Seppänen M, Raitakari O, Luotolahti M, Nuutila P, Wahren J and Knuuti J. (2002) Proinsulin C-peptide improves adenosine-induced myocardial vasodilation in Type 1 diabetes patents. *Circulation* submitted.

122. Kunt T, Forst T, Closs E, Wallerath T, Foerstermann U, Lehmann R, Pfuetzner A, Harzer O, Engelbach M and Beyer J. (1998) Activation of endothelial nitric oxide synthase (eNOS) by C-peptide. *Diabetologia* **41**, Suppl. 1, A176.

123. Cotter MA and Cameron NE. (2001) C-peptide effects on nerve conduction and blood flow in streptozotocin-induced diabetic rats: modulation by nitric oxide synthase inhibition. *Diabetes* **50**, A184.

124. Ido Y, Vindigni A, Chang K, Stramm L, Chance R, Heath WF, DiMarchi RD, Di Cera E and Williamson JR. (1997) Prevention of vascular and neural dysfunction in diabetic rats by C-peptide. *Science* **277**, 563-566.

125. Forst T, De La Tour DD, Kunt T, Pfützner A, Goitom K, Pohlmann T, Schneider S, Johansson BL, Wahren J, Löbig M, Engelbach M, Beyer J and Vague P. (2000) Effects of proinsulin C-peptide on nitric oxide, microvascular blood flow and erythrocyte Na^+,K^+-ATPase activity in diabetes mellitus type I. *Clin. Sci.* **98**, 283-290.

126. Tsimaratos M, Roger F, Mordasini D, Rousselot M, Bianchi M and Féraille E. (2001) C-peptide stimulates Na,K-ATPase through PKC pathway the medullary thick ascending limb. *Diabetologia* **44**, Suppl 1, A156.

127. Ohtomo Y, Aperia A, Sahlgren B, Johansson B-L and Wahren J. (1996) C-peptide stimulates rat renal tubular Na^+,K^+-ATPase activity in synergism with neuropeptide Y. *Diabetologia* **39**, 199-205.

128. Maiti S, Haupts U and Webb WW. (1997) Fluorescence correlation spectroscopy: diagnostics for sparse molecules. *Proc. Natl. Acad. Sci. USA* **94**, 11753-11757.

129. Rigler R, Pramanik A, Jonasson P, Kratz G, Jansson OT, Nygren P-Å, Ståhl S, Ekberg K, Johansson B-L, Uhlén S, Uhlén M, Jörnvall H and Wahren J. (1999) Specific binding of proinsulin C-peptide to human cell membranes. *Proc. Natl. Acad. Sci. USA* **96**, 13318-13323.

130. Henriksen JH, Tronier B and Bülow JB. (1987) Kinetics of circulating endogenous insulin, C-peptide, and proinsulin in fasting nondiabetic man. *Metabolism* **36**, 463-468.

131. Sjöberg S, Johansson B-L, Östman J and Wahren J. (1991) Renal and splanchnic exchange of human biosynthetic C-peptide in type 1 (insulin-dependent) diabetes mellitus. *Diabetologia* **34**, 423-428.

132. Polonsky K, Jaspan J, Pugh W, Cohen D, Schneider M, Schwartz T, Moossa AR, Tager H and Rubenstein AH. (1983) Metabolism of C-peptide in the dog. In vivo demonstration of the absence of hepatic extraction. *J. Clin. Invest.* **72**, 1114-1123.

133. Bratusch-Marrain PR, Waldhäusl WK, Gasic' S and Hofer A. (1984) Hepatic disposal of biosynthetic human insulin and porcine C-peptide in humans. *Metabolism* **33**, 151-157.

134. Faber OK, Hagen C, Binder C, Markussen J, Naithani VK, Blix PM, Kuzuya H, Horwitz DL, Rubenstein AH and Rossing N. (1978) Kinetics of human connecting peptide in normal and diabetic subjects. *J. Clin. Invest.* **62**, 197-203.

135. Anderson CJ and Welch MJ. (1999) Radiometal-labeled agents (non-technetium) for diagnostic imaging. *Chem. Rev.* **99**, 2219-2234.

136. Blok D, Feitsma RIJ, Vermeij P and Pauwels EJK. (1999) Peptide radiopharmaceuticals in nuclear medicine. *Eur. J. Nucl. Med.* **26**, 1511-1519.

137. Wilbur DS. (1992) Radiohalogenation of proteins: an overview of radionuclides, labeling methods, and reagents for conjugate labeling. *Bioconjug. Chem.* **3**, 433-470.

138. Westerberg G and Långström B. (1994) Labelling of proteins with ^{11}C in high specific radioactivity: [^{11}C]albumin and [^{11}C]transferrin. *Appl. Radiat. Isot.* **45**, 773-782.

139. Stöcklin G and Wester H-J. (1998) Strategies for radioligand development: Peptides for tumor targeting. In: *Positron emission tomography: A critical assessment of recent trends.* pp. 57-90; Edited by Gulyás B and Müller-Gärtner HW. Kluwer Academic Publishers, London.

140. Okarvi SM. (2001) Recent progress in fluorine-18 labelled peptide radiopharmaceuticals. *Eur. J. Nucl. Med.* **28**, 929-938.

141. Bolton AE and Hunter WM. (1973) The labelling of proteins to high specific radioactivities by conjugation to a ^{125}I-containing acylating agent. *Biochem. J.* **133**, 529-539.

142. Vaidyanathan G and Zalutsky MR. (1992) Labeling proteins with fluorine-18 using N-succinimidyl 4-[^{18}F]fluorobenzoate. *Nucl. Med. Biol.* **19**, 275-281.

143. Guhlke S, Coenen HH and Stöcklin G. (1994) Fluoroacylation agents based on small n.c.a. [^{18}F]fluorocarboxylic acids. *Appl. Radiat. Isot.* **45**, 715-727.

144. Vaidyanathan G and Zalutsky MR. (1994) Improved synthesis of N-succinimidyl 4-[^{18}F]fluorobenzoate and its application to the labeling of a monoclonal antibody fragment. *Bioconjug. Chem.* **5**, 352-356.

145. Vaidyanathan G and Zalutsky MR. (1995) Fluorine-18 labeled chemotactic peptides: a potential approach for the PET imaging of bacterial infection. *Nucl. Med. Biol.* **22**, 759-764.

146. Wester H-J, Hamacher K and Stöcklin G. (1996) A comparative study of N.C.A. fluorine-18 labeling of proteins via acylation and photochemical conjugation. *Nucl. Med. Biol.* **23**, 365-372.

147. Lang L and Eckelman WC. (1994) One-step synthesis of ^{18}F labeled [^{18}F]-N-succinimidyl 4-(fluoromethyl)benzoate for protein labeling. *Appl. Radiat. Isot.* **45**, 1155-1163.

148. Lang L and Eckelman WC. (1997) Labeling proteins at high specific activity using N-succinimidyl 4-[^{18}F](fluoromethyl) benzoate. *Appl. Radiat. Isot.* **48**, 169-173.

149. Ohtomo Y, Bergman T, Johansson B-L, Jörnvall H and Wahren J. (1998) Differential effects of proinsulin C-peptide fragments on Na$^+$,K$^+$-ATPase activity of renal tubule segments. *Diabetologia* **41**, 287-291.

150. Johnström P, Stone-Elander S and Duelfer T. (1994) [2'-^{18}F]-2-Oxoquazepam: Synthesis of a 5-(2-[^{18}F]fluorophenyl)-1,4-benzodiazepine-2-one. *J. Labelled Cpd. Radiopharm.* **34**, 147-156.

151. Kuhnast B, Dolle F, Vaufrey F, Hinnen F, Crouzel C and Tavitian B. (2000) Fluorine-18 labeling of oligonucleotides bearing chemically-modified ribose-phosphate backbones. *J. Labelled Cpd. Radiopharm* **43**, 837-848.

152. Hosteler ED, Edwards WB, Anderson CJ and Welch MJ. (1999) Synthesis of 4-[^{18}F]fluorobenzoyl octreotide and biodistribution in tumour-bearing Lewis rats. *J. Labelled Cpd. Radiopharm.* **42**, Suppl. 1, S720-S722.

153. Yngve U, Khan TS, Bergström M and Långström B. (2001) Labelling of octreotide using ^{76}Br-prosthetic groups. *J. Labelled Cpd. Radiopharm.* **44**, 561-573.

154. Sutcliffe-Goulden JL, O'Doherty MJ and Bansal SS. (2000) Solid phase synthesis of [^{18}F]labelled peptides for positron emission tomography. *Bioorg. Med. Chem. Lett.* **10**, 1501-1503.

155. Yu H-M, Chen S-T and Wang K-T. (1992) Enhanced coupling efficiency in solid-phase peptide synthesis by microwave irradiation. *J. Org. Chem.* **57**, 4781-4784.

156. Snyder WS, Cook MJ, Nasset ES, Karhausen LR, Howells GP and Tipton IH. (1975) *Report of the task group on reference man.* p. 109; Pergamon press, New York.

157. Polonsky KS, Licinio-Paixao J, Given BD, Pugh W, Rue P, Galloway J, Karrison T and Frank B. (1986) Use of biosynthetic human C-peptide in the measurement of insulin secretion rates in normal volunteers and type 1 diabetic patients. *J. Clin. Invest.* **77**, 98-105.

158. Flatt PR, Swanston-Flatt SK, Hampton SM, Bailey CJ and Marks V. (1986) Specific binding of the C-peptide of proinsulin to cultured B-cells from a transplantable rat islet cell tumor. *Biosci. Rep.* **6**, 193-199.

159. Zierath JR, Handberg A, Tally M and Wallberg-Henriksson H. (1996) C-peptide stimulates glucose transport in isolated human skeletal muscle independent of insulin receptor and tyrosine kinase activation. *Diabetologia* **39**, 306-313.

160. Gruppuso PA, Susa JB, Sehgal P, Frank B and Schwartz R. (1987) Metabolism and placental transfer of ^{125}I-proinsulin and ^{125}I-tyrosylated C-peptide in the pregnant rhesus monkey. *J. Clin. Invest.* **80**, 1132-1137.

161. Onkamo P, Väänänen S, Karvonen M and Tuomilehto J. (1999) Worldwide increase in incidence of Type I diabetes - the analysis of the data on published incidence trends. *Diabetologia* **42**, 1395-1403.